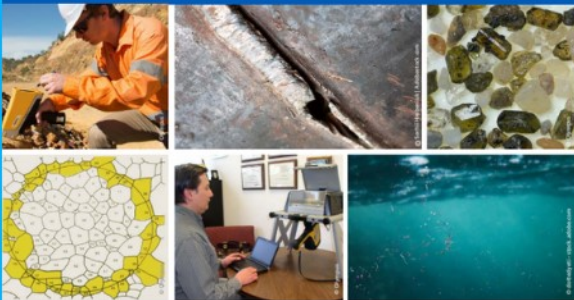# 2nd Advanced Optical Metrology Compendium

Advanced Optical Metrology

Geoscience | Corrosion | Particles | Additive
Manufacturing: Metallurgy, Cut Analysis & Porosity

EVIDENT
OLYMPUS

WILEY

The latest eBook from Advanced Optical Metrology. Download for free.

This compendium includes a collection of optical metrology papers, a repository of teaching materials, and instructions on how to publish scientific achievements.

With the aim of improving communication between fundamental research and industrial applications in the field of optical metrology we have collected and organized existing information and made it more accessible and useful for researchers and practitioners.

EVIDENT
OLYMPUS

WILEY

REVIEW

Engineering Halide Perovskite Crystals through Precursor Chemistry

Bo Li, David Binks,* Guozhong Cao,* and Jianjun Tian*

The composition, crystallinity, morphology, and trap-state density of halide perovskite thin films critically depend on the nature of the precursor solution. A fundamental understanding of the liquid-to-solid transformation mechanism is thus essential to the fabrication of high-quality thin films of halide perovskite crystals for applications such as high-performance photovoltaics and is the topic of this Review. The roles of additives on the evolution of coordination complex species in the precursor solutions and the resulting effect on perovskite crystallization are presented. The influence of colloid characteristics, DMF/DMSO-free solutions and the degradation of precursor solutions on the formation of perovskite crystals are also discussed. Finally, the general formation mechanism of perovskite thin films from precursor solutions is summarized and some questions for further research are provided.

1. Introduction

Organic–inorganic hybrid halide perovskite materials have the general formula ABX_3, where A is a monovalent organic cation (such as methylammonium (MA) or formamidinium (FA)), B = Pb, Sn, and X = Cl, Br, I. $CH_3NH_3PbI_3$ (MAPbI₃) was first reported by Weber in 1978.[1] Recent studies have demonstrated that the perovskites possess excellent semiconducting characteristics including large optical absorption coefficient,[2] small exciton binding energy,[3] long charge carrier diffusion lengths,[4] and defect-tolerant electronic properties.[5] Perovskite thin films with excellent crystallinity and low trap-state density can be obtained by low-temperature solution processes due to their low crystallization activation energy barrier.[6] Hybrid lead halide perovskites have emerged as a class of promising light-harvesting materials since the first use in dye-sensitized structure solar cells in 2009.[7] To date, perovskite-based solar cells (PSCs) with power conversion efficiencies (PCE) as high as 25.2% have been certified,[8] and a diverse range of solution process technologies, including one-step spin-coating,[9] sequential deposition,[10] and blade-coating[11] have been developed to fabricate high-quality perovskite thin films. Among them, one-step spin-coating from solution remains one of the most frequently-used deposition methods for the fabrication of high-efficiency perovskite devices.[12] However, early works on this one-step approach commonly reported incomplete coverage and needle-like morphology,[13] resulting in shunting and reduced light absorption in PSCs.

The general strategy toward improving the coverage of perovskite thin films is to increase nuclei density by accelerating the evaporation of solvents. For example, by the exposure of the wet film to excess amounts of antisolvent, such as toluene,[9] chlorobenzene,[13b] diethyl ether,[13c] or ethyl acetate[14] in a very short time (<1 s), fast perovskite crystallization is immediately induced in supersaturated precursor solutions, leading to the formation of highly uniform perovskite thin films with small crystalline grains. However, the very narrow time window makes this approach difficult operationally,[15] and is not compatible with scalable methods. On the other hand, retarded crystallization by control of the chemical coordination in the precursor solution has been explored to achieve high-quality thin films with enlarged grain size and reduced trap-state density.[15a,16] For all-solution fabrication processes, the nature of precursor solution not only impacts the nucleation rate and crystallization kinetics of perovskite crystals,[12f,14,17] but also influences the physical properties of the resulting perovskite thin films, such as the morphology,[18] crystallinity,[19] trap-state density,[17a,20] and charge carrier mobility.[21]

In this Review, we focus on present progress in the study of perovskite precursor solution chemistry and relate it to the formation of thin films from these solutions. First, we provide insights into the chemical nature of perovskite precursor solutions, followed by a discussion of the basic principles describing the formation of thin films. The effect of an additive strategy on both the coordination complexes in precursor solutions and perovskite crystallization is then discussed. In particular, we highlight the dependency of the final perovskite grains to the colloidal characteristics of the precursor solution. Finally, we summarize the general formation mechanism of perovskite

Dr. B. Li, Prof. J. Tian
Institute for Advanced Materials and Technology
University of Science and Technology Beijing
Beijing 100083, China
E-mail: tianjianjun@mater.ustb.edu.cn
Prof. D. Binks
School of Physics and Astronomy and Photon Science Institute
University of Manchester
Manchester M13 9PL, UK
E-mail: David.Binks@manchester.ac.uk
Prof. G. Cao
Department of Materials and Engineering
University of Washington
Seattle, WA 98195-2120, USA
E-mail: gzcao@uw.edu

The ORCID identification number(s) for the author(s) of this article can be found under https://doi.org/10.1002/smll.201903613.

thin films from precursor solutions and propose some questions to be addressed in the future.

## 2. Nature of Perovskite Precursor Solutions

2.1. Solute Coordination Interaction

Organic–inorganic hybrid lead halide perovskite precursor solutions are generally composed of stoichiometric mixtures of the organic (MAX or FAX, X = I, Br, and Cl) and inorganic lead source (PbX$_2$, X = I, Br, and Cl) in a polar aprotic solvent or mixed solvents,[22] in which Pb^{2+} would act as Lewis acid to coordinate with Lewis bases (DMF or DMSO).[13c] Lead (II) coordination chemistry has been studied extensively due to the stereochemical activity of its 6s^2 lone pair.[23] As shown in **Figure 1**a, by gradually increasing the MAI concentration in a PbI$_2$ solution, the complexation between PbI$_2$ and I$^-$ forms iodoplumbate coordination complexes of PbI$_3^-$ and PbI$_4^{2-}$, while absorption bands of PbI$_5^{3-}$ and PbI$_6^{4-}$ are not observed in the absorbance spectra.[24] Thus, PbI$_4^{2-}$ ions would be the final reactant in perovskite precursor solution. As depicted in Figure 1b, it can be deduced that the intercalation reactions of layered PbI$_2$ with I$^-$ would be expected due to the low activation energy, and the Pb—I chemical bonds of PbI$_2$ would be broken and reconstructed to form a series of iodoplumbate coordination complexes, until reaching the equilibria between PbI$_2$, PbI$_3^-$, and PbI$_4^{2-}$ as described in Equations (1) and (2)[25]

$$PbI_2 + I^- \leftrightarrow PbI_3^- \, (K_1) \tag{1}$$

$$PbI_3^- + I^- \leftrightarrow PbI_4^{2-} \, (K_2) \tag{2}$$

where K is equilibrium constant. As a result, the mole ratio of PbI$_2$: I$^-$ determines the shift of the equilibria, as well as the species of coordination complexes in precursor solutions.

Recently, significant progress has been made in the in-depth understanding of the nature of perovskite precursor solutions. Yan and co-workers revealed the colloidal properties of perovskite precursor solutions.[26] As shown in Figure 1c, by analyzing the size distribution of the colloidal particles in the precursor solutions with different ratios of organic and inorganic components, they found that the excess MAI in the precursor solution reduced the size of colloidal particles. These results are consistent with the coordination of layered PbI$_2$ with I$^-$, and indicates that the coordination complex species in the precursor is determined by the solution equilibria in Equations (1) and (2). A recent study investigated the chemical equilibrium in perovskite precursor solutions and tried to determine whether the iodoplumbate coordination complexes in precursor solutions were correlated with the density of charge recombination centers in final perovskite thin film.[27] They confirmed that there were high concentrations of PbI$_2$, PbI$_3^-$, and PbI$_4^{2-}$ in perovskite precursor solutions, and the concentration of PbI$_4^{2-}$ showed unique correlation to the density of charge recombination centers in the perovskite thin films produced. However, the stoichiometric and structural information of colloidal particles (intermediate phase) in perovskite precursor solution are experimentally difficult to know due to the metastability of the
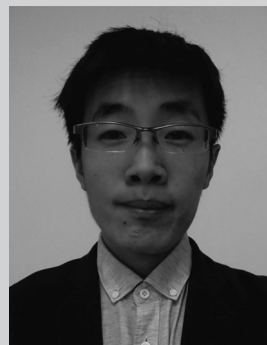
Bo Li received his Ph.D. degree from the University of Science and Technology Beijing in 2019 supervised by Prof. Jianjun Tian. His study was focused on the fabrication of highly efficient perovskite solar cells in the Laboratory of Optoelectronic Materials and Devices. His research focuses on understanding the formation mechanism of solution-processed perovskite.

Guozhong Cao is Boeing-Steiner Professor of materials science and engineering, chemical engineering, and adjunct professor of mechanical engineering at the University of Washington (Seattle). His current research is focused on chemical processing of nanomaterials for energy-related applications including solar cells, rechargeable batteries, supercapacitors, and hydrogen storage.

Jianjun Tian is a professor in Institute for Advanced Materials and Technology, University of Science and Technology Beijing (USTB). He received his Ph.D. in USTB in 2007. During 2011–2012, he studied in University of Washington. He was selected as new century excellent talents of Ministry of Education in 2013, built the Laboratory of Optoelectronic Materials and Devices in 2016, and was nominated as director of Functional Materials Institute, USTB in 2015 and vice-dean of Institute for Multidisciplinary Innovation, USTB in 2019. Current research focuses on quantum dots and perovskites, and their applications, including solar cells, light emitting and photodetectors.

precursor,[6b] and there is a debate on whether the precursor has crystalline structure or amorphous phase. The gel-like scattering halo at low q values of nanometric length scale mesophase were confirmed by in situ time-resolved grazing-incidence wide-angle X-ray scattering (GIWAXS) measurements at initial spin coating process, while the scattering halo dynamically

**ADVANCED
SCIENCE NEWS**

www.advancedsciencenews.com

NANO · MICRO

small

www.small-journal.com
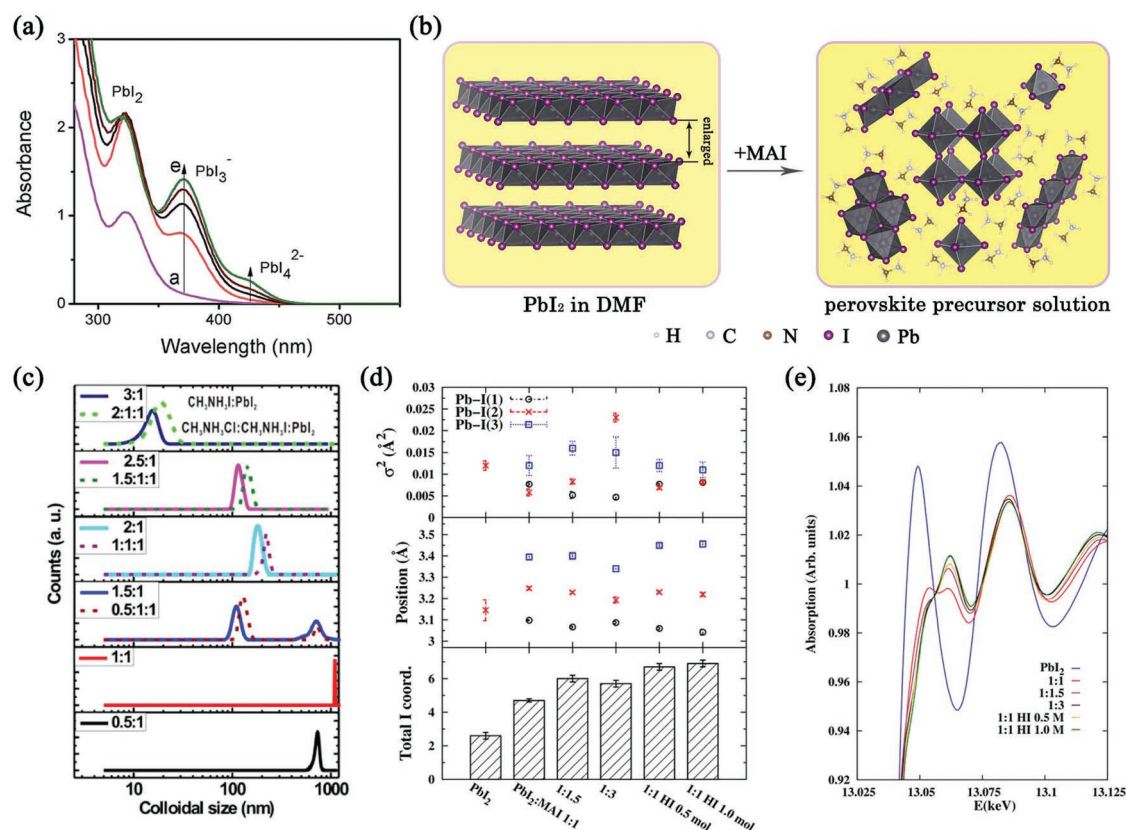
Figure 1. a) Absorption spectra of 250×10^{-6} M PbI_2 solution in DMF with increasing concentration of MAI from 6 to 24×10^{-3} M. Reproduced with permission.[24] Copyright 2015, The Royal Society of Chemistry. b) Schematic illustration of the formation of iodoplumbate coordination complexes in precursor solution due to the complexation between PbI_2 and I^-; c) Size distribution by dynamic light scattering. Reproduced with permission.[26] Copyright 2015, American Chemical Society. d) Real-space extended X-ray absorption fine structure (EXAFS) fit parameters. The top panel plots the correlated Debye–Waller factor (σ^2), the middle panel the Pb-I components' positions from the absorbing Pb atom, and the bottom panel the total iodide coordination number of the Pb atoms in solution. Note that disorder increases as the value of σ^2 increases and the Pb atoms in both PbI_2 and $MAPbI_3$ exhibit octahedral iodide coordination (PbI_6). e) Pb L-III edge X-ray absorption near edge structure (XANES) spectra of the measured samples. d,e) Reproduced with permission.[28] Copyright 2017, American Chemical Society.

shifts to higher q values as solvent evaporation, indicating the transformation of the solution into the intermediate phase with the higher order structure.[6b,28]
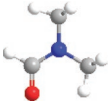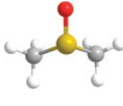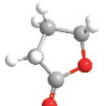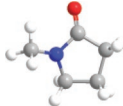
To further explore the exact structure of those coordination complexes, Sharenko and co-workers investigated the local structure of perovskite precursor solution by using X-ray absorption spectroscopy.[29] They found that the total iodide coordination number increased as the concentration of MAI increases from 1 to 1.5 M (see Figure 1d). Meanwhile, increasing values of the Debye–Waller factor σ^2 for the Pb-I (2) and Pb-I (3) components indicated more structural disorder for the coordination complexes. By comparing the Pb—I bond lengths in the iodoplumbate complexes and tetragonal $MAPbI_3$ structure, the lack of a comparable Pb—I bond lengths implied that the iodoplumbate complexes in perovskite precursor were composed of extended Pb-I fragments rather perovskite structure. Furthermore, a large shoulder at $\approx$13 052 eV in the X-ray absorption near edge structure data was observed in the case of the mole ratio of 1:1 for MAI: PbI_2 (see Figure 1e), which was attributed to the presence of Pb-O coordination from the residual coordination complex of PbI_2-DMF. It suggests that there may be an I-poor environment for coordination complexes in the normal perovskite precursor solution. Hence, it was suggested that excess I^- should be introduced to the perovskite precursor solution to avoid the formation of I-deficient perovskite structures with deep electron and holes traps.[30]

2.2. Solvent Effect

Due to the poor solubility of inorganic halide lead salts, precursor solutions are often limited to strongly polar aprotic organic solvents.[31] **Table 1** summaries the typical physical and chemical properties of the conventional organic solvents used for perovskite precursor solutions. In general, the boiling point and vapor pressure of the solvents determine the evaporation rate. Meanwhile, the impact of viscosity on the film formation cannot be ignored, the solvents with high viscosity have bad wetting on substrates to cause heterogeneous traces.[15a,32] The choice of solvent also affects the properties of the solution in a number of other ways. The presence of solvent-solute coordination in precursor solutions is widely observed due to the Lewis base characteristics of polar aprotic organic solvents.[19a,b,24b,29] Although the dielectric constant of a solvent reveals the

ADVANCED
SCIENCE NEWS
www.advancedsciencenews.com

NANO · MICRO
small
www.small-journal.com

Table 1. Typical physical and chemical properties of common organic solvents used for perovskite precursor solutions.

Solvent	N, N-dimethylformamide (DMF)	Dimethyl sulfoxide (DMSO)	γ-Butyrolactone (GBL)	N-Methyl-2-pyrrolidone (NMP)	Acetonitrile (ACN)
Chemical structure					
Chemical formula	C_3H_7NO	C_2H_6OS	$C_4H_6O_2$	C_5H_9NO	C_2H_3N
Boiling point (°C)	153	189	204	202	82
Vapor pressure (mmHg, 20 °C)	2.7	0.42	1.5	0.29	72.8
Viscosity (mPa s^{-1}, 20 °C)	0.92	1.996	1.75	1.67	0.369
Dielectric constants (20 °C)	38.3	47.2	41.7	32.2	36.6
Dipole moment (D)	3.86	3.96	4.27	4.09	3.92
Donor number (kcal mol^{-1})	26.6	29.8	17.8	27.3	14.1

chemical polarity,[33] there are some discrete results that could affect the estimating accuracy of the solvent-solute coordination by only considering the dielectric constants.[33b,34] For example, the crystallization of perovskite was readily occurred in precursor solution with the solvent of acetonitrile,[24b,32] regardless of its comparable dielectric constants relative to the commonly used N, N-dimethylformamide (DMF) solvent (see Table 1).

To elucidate the role of the Lewis basicity of solvents in perovskite precursor solutions, Hamill and co-workers quantified the dissolving ability of solvents by using Gutmann's donor number D_N,[24b] the values of which represent the ability of the solvents to solvate cations and Lewis acids.[34] They found that solvents with high D_N tended to coordinate with Pb^{2+} centers, which inhibits the formation of iodoplumbate complexes and retards the perovskite crystallization. In contrast, solvents with low D_N exhibited a weak affinity to Pb^{2+} and thus facilitated the formation of iodoplumbate complexes, which provides an environment for the growth of perovskite single-crystals. Hence, the solvation ability plays a critical role in determining the components of the perovskite precursor solution as well as the perovskite crystallization.

It is now clear that there is a competition between I^- and solvent molecules to coordinate with PbI_2, which determines the coordination complex species in perovskite precursor solutions. **Figure 2** shows schematic illustrations of the coordination complex species in perovskite precursor solutions. When the solvation ability of solvent is low, the affinity of PbI_2 toward I^- would be higher than that of PbI_2 toward solvent molecules, so it facilitates the formation of iodoplumbate complexes PbI_3^-, and PbI_4^{2-} (which are requisite to perovskite formation) or even the perovskite single-crystals. In contrast, a strong coordination solvent would instead induce the replacement of I^- from Pb^{2+} coordination sites by solvent molecules, and this intermediate phase in the precursor solution would strongly suppress the subsequent perovskite crystallization. In addition, the solubility of the coordiantion complexes could be related to the temperature of precursor solutions, the lower solvation ability of solvent is expected when reducing the iodoplumbate complexes solubility at a certain temperature, in turn resulting in the formation of iodoplumbate complexes with higher order structures. $MAPbX_3$ perovskites show an inverse temperature solubility behavior in certain solvents, high-quality single crystals of
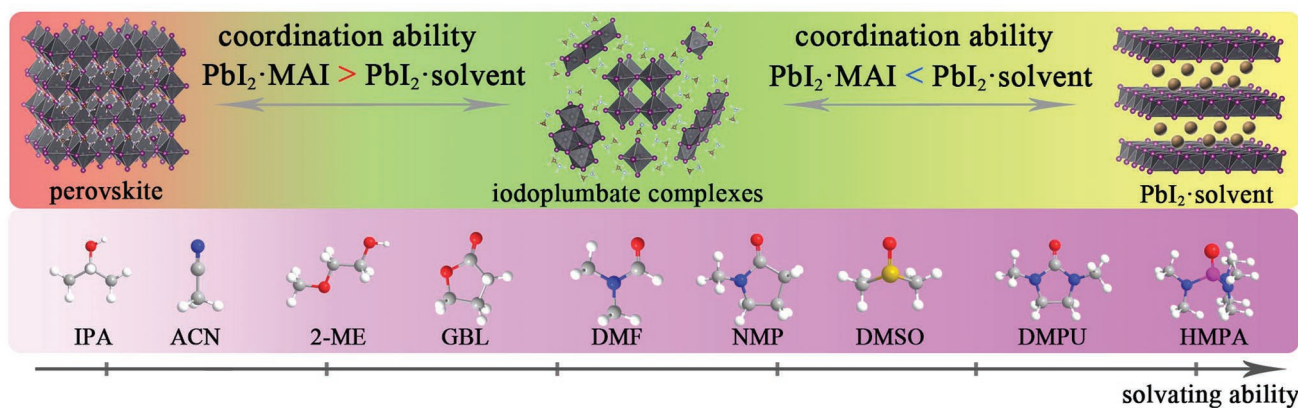
Figure 2. Schematic illustration of equilibria among perovskite, iodoplumbate complexes, and PbI_2·solvent based on the competition between I^- and solvent to coordinate with PbI_2.

**ADVANCED
SCIENCE NEWS**

www.advancedsciencenews.com

NANO · MICRO
small

www.small-journal.com

MAPbBr$_3$ and MAPbI$_3$ forming at an elevated temperature in DMF and gamma-butyrolactone (GBL) solutions, respectively.[35] A completely reversible chromatic variation ranging from yellow to black of the perovskite precursor solution in GBL under different temperatures was also reported.[36] These results further confirm that changes in coordination complex species occur due to shifts of equilibria among the iodoplumbate complexes.

3. Controlling Precursor Solution Characteristics for Perovskite Crystallization

3.1. Perovskite Crystallization from Additive-Free Precursor Solutions

According to classical nucleation theory, perovskite crystallization from a precursor solution is only expected to occur upon reaching supersaturation. As mentioned in Section 2.2, the most common solvents used to prepare perovskite precursor solution, including DMF and DMSO, have the high boiling point and low saturated vapor pressure (see Table 1), making them difficult to rapidly evaporate from the wet precursor thin films during perovskite crystallization.[37] As a result, residual solvent molecules undergo secondary bonding with solutes,[9,13d,31,38] which degrades the crystal morphology and causes poor coverage of the thin films. To allow for the formation of continuous and compact perovskite films, trapped solvent molecules should be removed or at least minimized.[13d,28a] In this regard, choosing the solvents with high saturated vapor pressure will produce compact perovskite thin films. For example, employing volatile 2-methoxyethanl (2-ME) as the solvent can achieve rapid drying of the wet thin films with an enhanced nucleation rate, leading to the more compact perovskite thin films with a smaller size of crystals.[39] However, due to the solvation effect in solvent-solute coordination complexes, it is hard to achieve the complete removal of solvents during the spin coating process, so it is difficult to obtain pinhole-free thin films using this strategy.
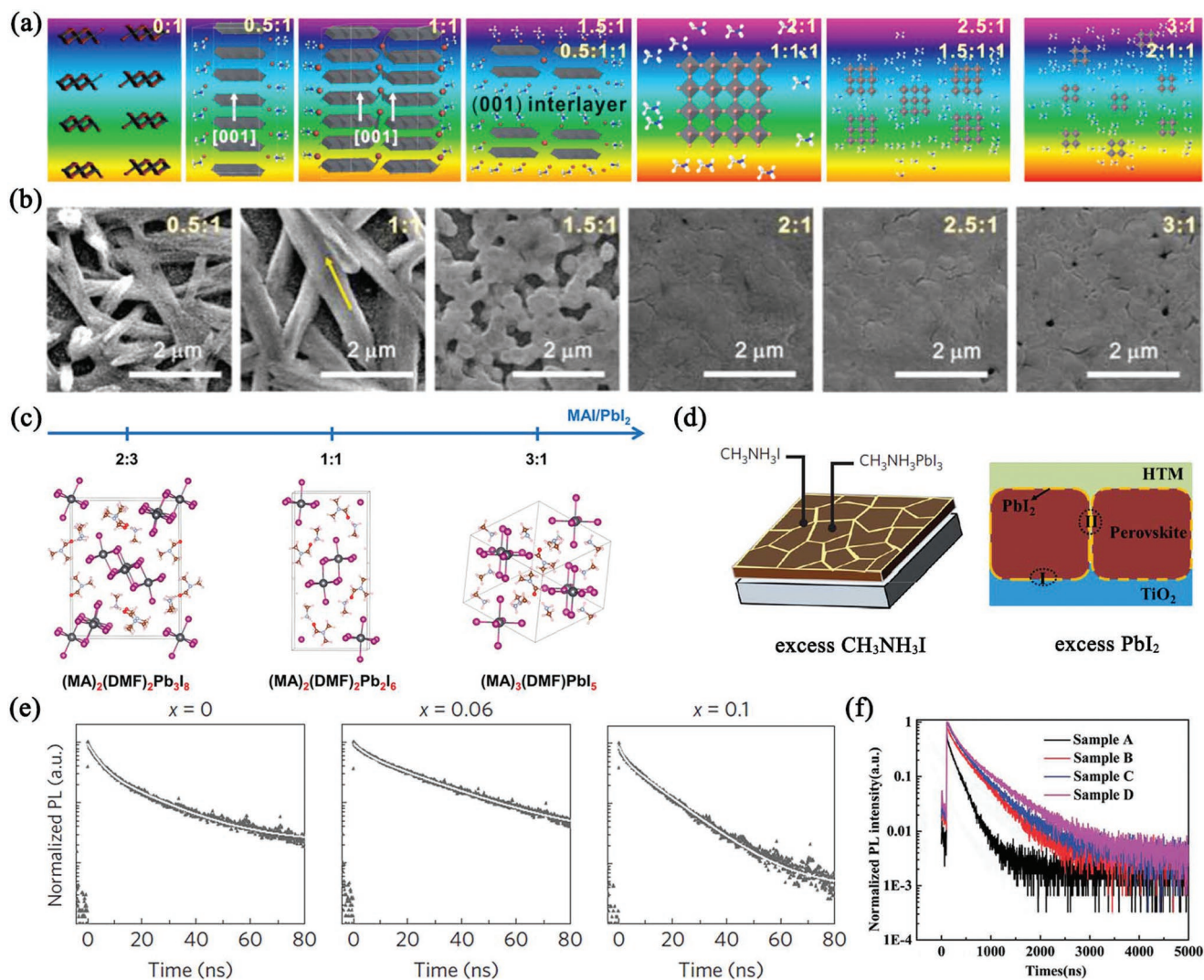
The coordination complex species in the precursor solutions also affects the perovskite crystallization process and the final crystal morphology. Yan and co-workers proposed the following formation mechanism involving a colloidal intermediate phase (see **Figure 3**a): 1) intercalation of DMF into layers of PbI$_2$, resulting in 1D pieces along (001) plane with some dangling bonds at (001) plane edges; 2) the incorporation of MAI triggering a selective coordination interaction with PbI$_2$ from the (001) plane edges, leading to the formation of trigonal PbI$_2$ with a nanorod micro-morphology; 3) a slight increase in the amount of MAI induces a nonselective coordination mode, with MAI now acting as solvent to dissolve and coordinate with trigonal PbI$_2$ toward a tetragonal transformation for maximum coordination, and forms a quasi-tetragonal soft framework.[26] This mechanism results in smaller colloidal cluster sizes in the precursor solution for higher MAI content. As shown in Figure 3b, PbI$_2$ dominates the perovskite crystallization process when the mole ratio of MAI: PbI$_2$ is below 1:1, resulting in needle-like perovskite crystals.[26] Notably, this needle-like morphology is also observed in the case of the mole ratio of MAI: PbI$_2$ is 1: 1, indicating that MAI molecules may not fully coordinate

with PbI$_2$ in normal perovskite precursor solution, which is consistent with a coordination interaction between PbI$_2$ and DMF, as suggested in Section 2.1. The equilibria between PbI$_2$, PbI$_3^-$, and PbI$_4^{2-}$ shift to higher coordinated plumbate species in the case of stoichiometric excess of MAI in the precursor solution, which could retard the fast crystallization of PbI$_2$ and improve the homogeneity of the perovskite thin films. Indeed, the presence of three different intermediate phases based on the ratios of MAI and PbI$_2$ have been confirmed.[40] As shown in Figure 3c, both PbI$_2$-rich (MA)$_2$(DMF)$_2$Pb$_3$I$_8$ and stoichiometric (MA)$_2$(DMF)$_2$PbI_6 phases contain face-sharing PbI$_6$ octahedral, which have a high anisotropy in the surface energy of growth, so that the resulting crystals tend to form needle-like morphology. In the case of MAI-rich (MA)$_3$(DMF)PbI$_5$ phase, isolated corner-sharing PbI$_6$ octahedra with higher symmetry are observed, which tends to eliminate the needle-like crystals. In addition, the effects of cation species (MA$^+$, FA$^+$, and Cs$^+$) in precursor solutions on the perovskite crystallization kinetics have been partly illustrated. For example, Xu and co-workers reported that MA/FA cation ratio would affect the surface energy of the mixed perovskites, leading to the variation of preferential orientation in mixed-cation perovskites.[41]

Although the excess MAI in precursor solution results in an intermediate phase with higher symmetry and improves the morphology of the final perovskite thin films, the effect of the remnant MAI in the final perovskite thin films is still under debate. As shown in Figure 3d, both the introduction of excess MAI and PbI$_2$ in the precursor solution result in the separation and concentration along grain boundaries, which would act as a grain boundary healing layer to suppress nonradiative recombination.[42] As a result, the lifetime of carriers was significantly increased in comparison with the normal perovskite thin films (see Figure 3e,f).[42b,43] It is generally accepted that MAI-rich perovskite thin films show more complete conversion of PbI$_2$ into the perovskite phase, while both charge carrier transport and electron injection are limited due to the accumulation of the organic component. Alternatively, PbI$_2$-rich perovskite thin films have reduced halide vacancy concentration and change the preferred orientation of the perovskite crystal, leading to higher efficiency solar cells.[44]

3.2. Fast Nucleation

As described in Sections 2.1 and 2.2, because of the inadequate complexation between Pb^{2+} and I$^-$ and the lower solubility of the inorganic component in the perovskite precursor solution, the 1D Lewis adduct of the PbI$_2$·DMF (coordinates with some MAI) would precipitate from the precursor solution prior to perovskite crystallization under an uncontrolled perovskite solidification, leading to the compositional segregation of MAI.[59] Then the PbI$_2$·DMF complex reacts with the segregated MAI to form perovskite crystals with the needle-like morphology as commonly reported in the literatures.[20,60] According to classical nucleation theory, shortening the time for the precursor solution to reach the state of supersaturation leads to an increased nucleation rate, which would produce numerous small initial nuclei and give rise to the improved coverage of thin films.[45] In this regard, the accelerated perovskite
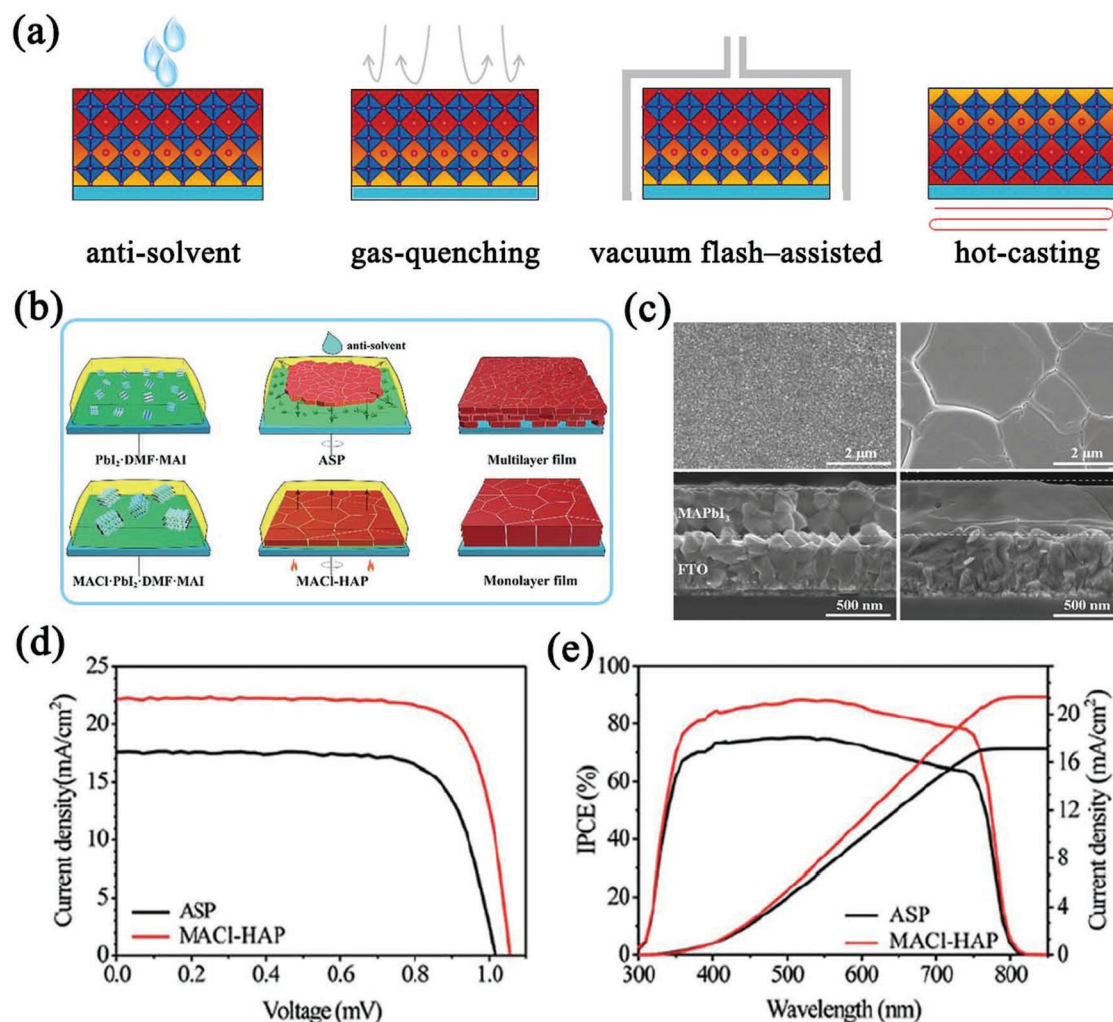
**ADVANCED
SCIENCE NEWS**

www.advancedsciencenews.com

NANO · MICRO

small

www.small-journal.com

Figure 3. a) Possible organic–inorganic coordination products at different MAI: PbI$_2$ ratios in the perovskite precursors. b) SEM micrographs of the calcined thin films with different ratio of MAI:PbI$_2$. a,b) Reproduced with permission.[26] Copyright 2015, American Chemical Society. c) Crystal structures of three intermediate phases: PbI$_2$-rich (MA)$_2$(DMF)$_2$Pb$_3$I$_8$, stoichiometric (MA)$_2$(DMF)$_2$Pb$_2$I$_6$, and MAI-rich (MA)$_3$(DMF)PbI$_5$. Reproduced with permission.[41] Copyright 2017, American Chemical Society. d) Schematic representation of the CH$_3$NH$_3$PbI$_3$ perovskite thin films with grain boundary healing layer and self-induced passivation by excess CH$_3$NH$_3$I and excess PbI$_2$, respectively. Reproduced with permission.[44] Copyright 2014, American Chemical Society. e) Time-resolved PL spectra for the MAPbI$_3$ perovskite films with different molar concentration of MAI precursor. d,e) Reproduced with permission.[43a] Copyright 2016, Nature Publishing Group. f) Time-resolved photoluminescence (TRPL) spectra of perovskite with different compositions, sample A: no PbI$_2$ was observed on the surface; sample B: observable white phase of PbI$_2$ formed on the perovskite surface; sample C: increase of PbI$_2$ on the surface; sample D: over excess of PbI$_2$ formed on perovskite surface. Reproduced with permission.[43b] Copyright 2017, Wiley-VCH.

nucleation though the fast removal of solvents could effectively avoid the needle-like morphology of perovskite thin films.

Figure 4a schematically illustrates the present strategies on the rapid removal of solvent from the wet films, including anti-solvent extraction,[13b] gas-quenching,[46] and vacuum-assisted drying.[47] Among them, the mechanism of promoting solvent evaporation is typical for each kind of method. Briefly, the solvent molecules are abruptly extracted from the top to bottom of the film, resulting in a high nucleation density followed by perovskite crystallization. However, the fast crystallization of perovskite starts on the surface of the wet thin films, which may prevent the subsequent infiltration of antisolvent or gas flow, leading to the insufficient extraction of solvent in the bottom

of the wet thin films. By contrast, as depicted in Figure 4b,[48] the heat-assisted process provides a bottom-up crystal growth model due to the heat transfer from the substrate. The initial perovskite crystallization would then be induced from the precursor solution/substrate liquid–solid interface as heterogeneous nucleation. For example, our previous work confirmed that there were many shrinkage voids in the bottom of the perovskite thin films prepared by the antisolvent method, while the compact monolithic perovskite thin films were obtained by heat-assisted process strategy (see Figure 4c).[48] As shown in Figure 4d,e, a PCE of 18.34% for monolithic perovskite thin film based PSCs was obtained, in which the improvement of PCE was attributed to the enhanced J_{sc}.

**ADVANCED
SCIENCE NEWS**
www.advancedsciencenews.com

NANO · MICRO
small
www.small-journal.com

Figure 4. a) Schematic illustration of the strategies used to rapidly remove the solvents in perovskite precursors: antisolvent extraction, gas-quenching, vacuum-assisted drying, and hot-casting method; b) Schematic diagram of the formation of the multilayer and monolithic MAPbI$_3$ films by antisolvent process (ASP) and MACl–heat-assisted process (MACl-HAP). c) Top-view and cross-sectional SEM images of perovskite thin films prepared by ASP (left) and MACl-HAP (right); current density–voltage curve d) and incident photon-to-current conversion efficiency spectrum. e) of PSCs prepared by MACl–HAP and ASP. b,e) Reproduced with permission.[49] Copyright 2017, The Royal Society of Chemistry.

For the heat-assisted deposition method, the solvent evaporation rate is greatly affected by the temperature of substrates or precursor solutions, which shows great potential toward the future scalable fabrication by taking the advantage of uniformly controlling the supersaturation degree in a large area.[11b,49] However, the temperature choice has to be limited to avoid the thermal decomposition of produced perovskite films, so the degree of precursor solution supersaturation is usually lower compared to the antisolvent method. Alternatively, the solute diffusion rate would continuously increase, when the substrate is maintained above the crystallization temperature,[50] which promotes crystal growth and facilitates the formation of compact perovskite thin films with enlarged grain size. In fact, perovskite thin films with millimeter-scale crystalline grains have been reported by spin-coating the hot precursor solution (70 °C) onto the heated substrates maintained at 190 °C (see **Figure 5**a,b).[50,51] The resulting thin films exhibit lower nucleation density at first glance, while further

study revealed that the millimeter scale grains were also composed of polycrystalline microstructure with a grain size of <500 nm, instead of single-crystalline domains as shown in Figure 5c.[45a]

On the basis of this understanding of the heat-assisted spin coating method, the community has witnessed remarkable progress toward future scalable fabrication of PSCs,[19b,49,52] in which the continuous perovskite thin films can be prepared by balancing the competition between the solvent evaporation rate, solute diffusion rate, and crystal growth rate. Figure 5d schematically depicts the blade coating process based on heat-assisted method. The meniscus precursor solution edge appears between the hot substrate (typically 70–145 °C) and an upper plate, which constrains the diffusion of perovskite precursor solution due to capillary action.[53] As solvent evaporates, the meniscus at the edge drives an outward convective flow and the perovskite solute moves toward the solid/liquid boundary. As a result, the blade coating method requires the
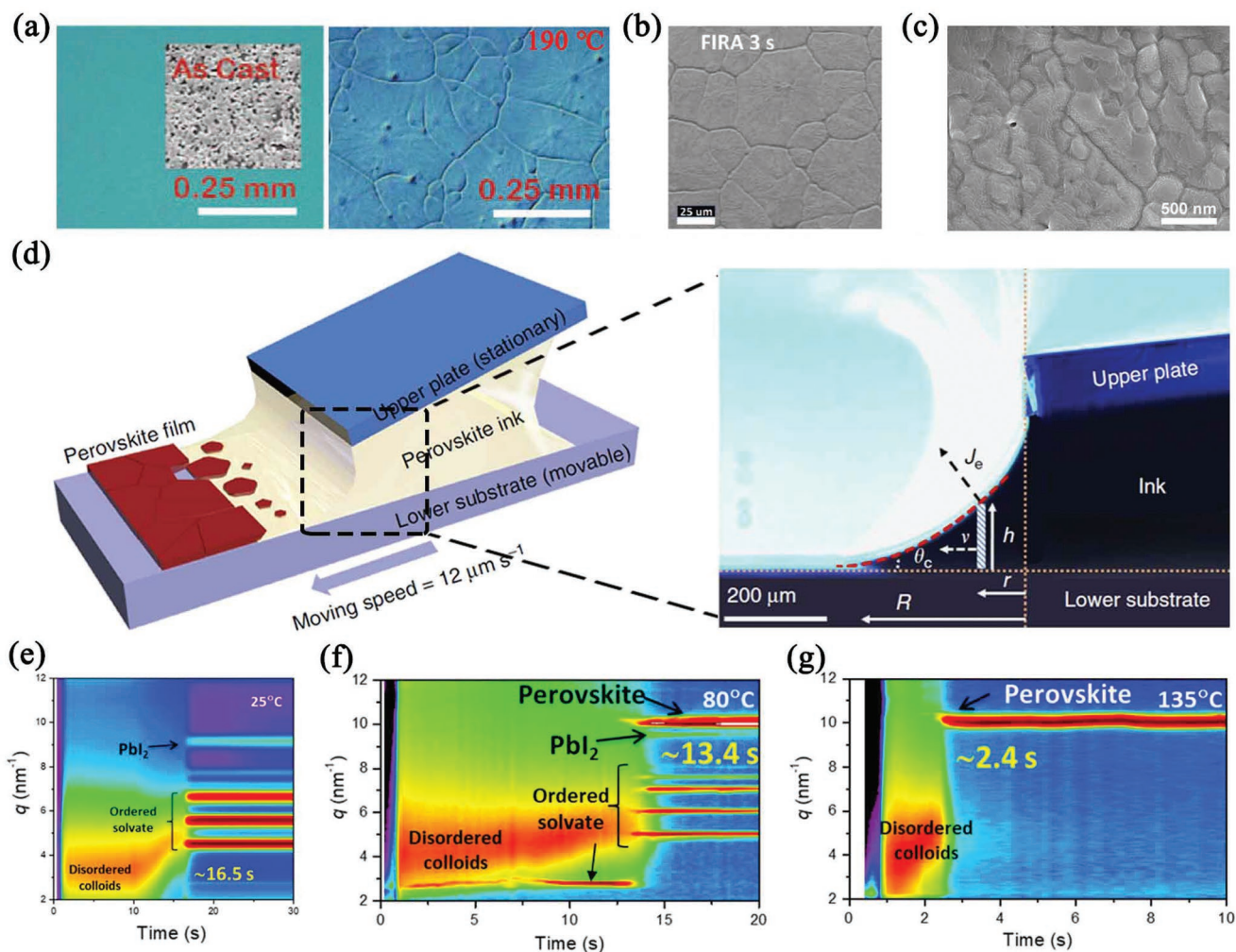
Figure 5. a) Optical micrographs of perovskite grains with the casting solution maintained at 190 °C. Reproduced with permission.[51] Copyright 2015, American Association for the Advancement of Science. b) Top view of FIRA-annealed perovskite films for annealing of 3 s. Reproduced with permission.[52] Copyright 2018, Wiley-VCH. c) SEM images of the $CH_3NH_3PbI_3$ large grain-cluster film at magnifications of 75 000X. Reproduced with permission.[46] Copyright 2017, Science China Press and Springer-Verlag GmbH Germany. d) Schematic illustration of the meniscus-assisted solution printing (MASP) of large-grained perovskite thin films and optical micrograph of the side-view meniscus ink confined between a lower flat, movable substrate and an upper stationary plate. Reproduced with permission.[54] Copyright 2017, Nature Publishing Group. In situ GIWAXS performed during blade-coating at e) 25 °C, f) 80 °C, and g) 135 °C. Reproduced with permission.[55] Copyright 2018, American Chemical Society.

exact control of the substrate temperature and blade-coating speed. With the aid of in situ time-resolved grazing incidence wide-angle X-ray scattering with a 0.1 s time resolution, the heat-assisted blade-coating process at different stages was studied.[54] It demonstrated the formation of PbI_2-rich intermediate phases, and the PbI_2 phase was clearly observed in the crystalline solvates at low temperature (below 80 °C) (see Figure 5e), which tended to form needle-like perovskite crystals. It is consistent with the literature that PbI_2 would dominate the perovskite crystallization process.[13d,55] The competition among solvate intermediate phases, PbI_2 phase and perovskite phase was increased at the higher temperature (80–100 °C) (see Figure 5f), resulting in a mixture of needle-like and compact thin film morphologies. Further increasing the temperature above 100 °C led to the direct conversion of the colloidal precursor to the perovskite phase, and the neither intermediate phase nor PbI_2 phase was observed during the extremely

rapid solidification process (see Figure 5g). Finally, equiaxed perovskite grains were achieved, while the large and uniform-looking regions at high temperature were found to comprise of a polycrystalline microstructure instead of single grains. These results indicate that the grain size of perovskite thin films deviates from the classic nucleation theory in the supersaturation degree-dependency of grain size.

3.3. Retarding Crystallization

Significant evidence in the literatures has pointed to the presence of intermediate phases prior to perovskite crystallization,[9,13c,56] indicating that perovskite crystallization involves multistep phase transitions. With this in mind, the incorporation of additives with strong coordination ability toward PbI_2 in the perovskite precursor solution would be expected to reconstruct

ADVANCED
SCIENCE NEWS
www.advancedsciencenews.com

NANO · MICRO
small
www.small-journal.com
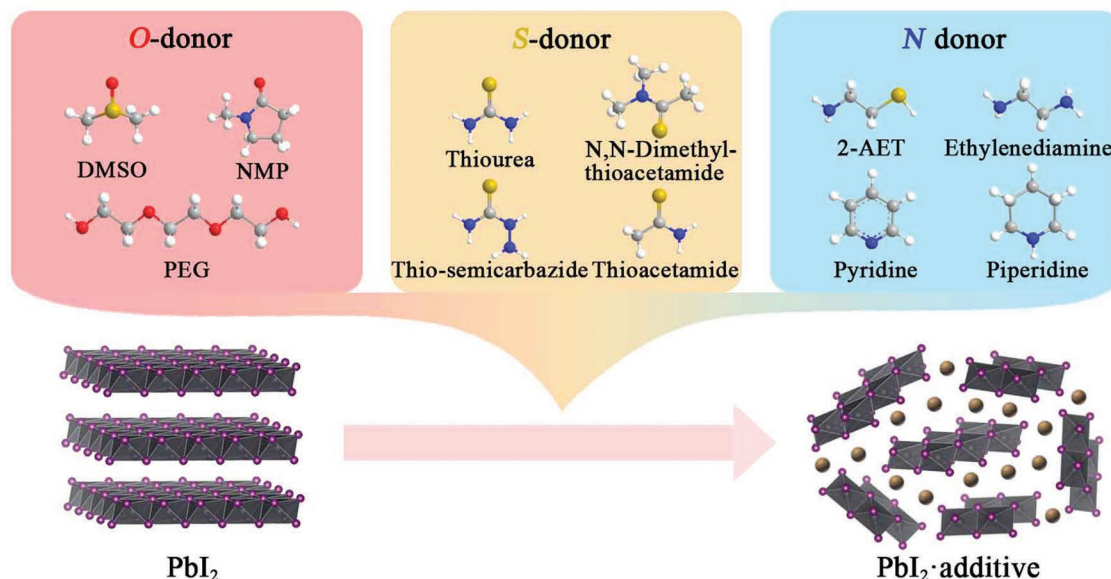
Figure 6. Schematic illustration of the formation of the PbI$_2$·complexes by Lewis acid–base coordination process with the additives based on oxygen-, sulfur-, and nitrogen-donor ligands.

the coordination interaction and structure of iodoplumbate complexes, so that the perovskite crystallization kinetic could be controlled. In particular, it is expected that the stronger the coordination ability of the additives in the precursor solution, the slower the crystallization of PbI$_2$ before that of the perovskite.
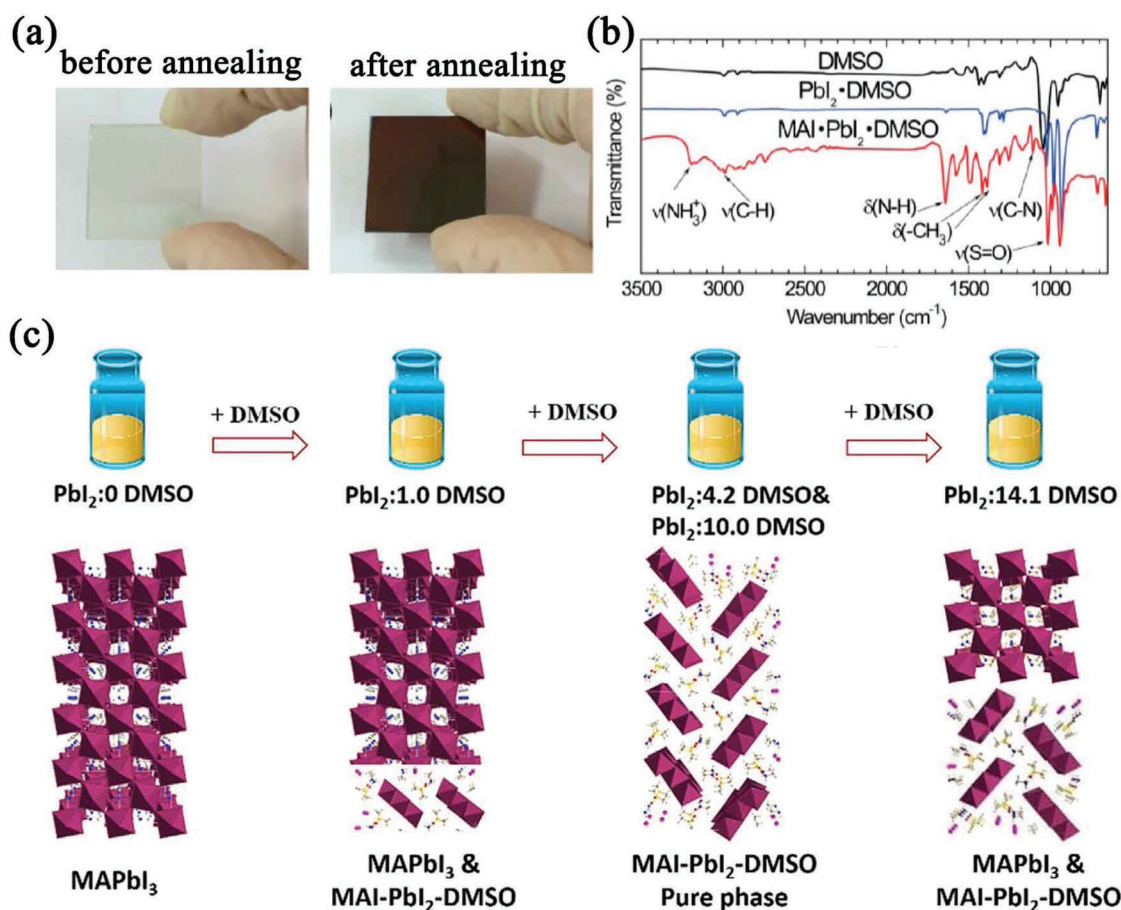
Studies of the co-ordination of various oxygen-, sulfur-, and nitrogen-donor ligands with Pb(II) Lewis acid have been widely reported.[23d,57] **Figure 6** summarizes the common additives used in perovskite precursor solutions. According to their functional groups, the additives are divided into three categories: O-donor, S-donor, and N-donor. Pb(II) is known as borderline soft in the hard and soft acid–base.[58] The donor ability of the ligands toward PbI$_2$ is in an order of S-donors > O-donors > N-donors. It can be deduced that the competition between the PbI$_2$·MAI complex and the PbI$_2$·additive complex would greatly affect the coordination complex species in the perovskite precursor solutions. By replacing the coordinated solvents molecules with the molecules of the additives would lead to the formation of the more stable intermediate phase so as to retard the perovskite crystallization.

The formation of intermediate phases with additives during the solidification of perovskite would directly determine its crystallization.[16a,c,17a,59] For the most commonly used additive of DMSO, the MAI·PbI$_2$·DMSO coordination complex was formed by the coordination interaction among Lewis base DMSO, MAI, and Lewis acid PbI$_2$ via C=O and N−H bonds in DMSO, which was revealed by the Fourier transform infrared spectroscopy (FTIR) (see **Figure 7**a,b). XRD patterns confirmed the MAI·PbI$_2$·DMSO coordination complex with a larger lattice constant, rather than PbI$_2$, MAI, PbI$_2$·DMSO or perovskite.[9] Although it was known that the DMSO could coordinate with PbI$_2$ to form a PbI$_2$(DMSO)$_2$ complex,[9,60] the systematic study on the effects of the intermediate phases on perovskite growth are still less-understood. Recently, Bai and co-workers investigated the effect of the intermediate phase induced

by DMSO on the perovskite crystallization.[38a] According to the DMSO/DMF ratio in perovskite precursor solutions, the formation of pure perovskite, a mixture of perovskite and MA$_2$Pb$_3$I$_8$(DMSO)$_2$, and pure MA$_2$Pb$_3$I$_8$(DMSO)$_2$ in wet films have been confirmed (see Figure 7c). In addition, only the pure phase of MA$_2$Pb$_3$I$_8$(DMSO)$_2$ was found to grow along [110] to induce aligned perovskite crystals with few horizontal grain boundaries.

Apart from the effect of the additive strategy on retarding the perovskite crystallization, we also found that the stability of the coordination complexes was correlated with the coordination ability of Lewis base additives, which showed a strong link to the quality of the perovskite thin films.[19a,61] As depicted in **Figure 8**a, we extracted the solvates from the perovskite precursor solutions to reveal the coordination interaction between the perovskite precursor salts and additives. In the case of the additive-free perovskite precursor solution, the solvate divided into a white MAI upper layer and a yellow PbI$_2$ bottom layer, indicating there was weak interaction between MAI and PbI$_2$. Interestingly, a transparent yellow gel complex without separated layers was formed for the perovskite precursor solution with 2-aminoethanethiol (2-AET) additive, implying that 2-AET in perovskite precursor solution possesses a strong coordination interaction to bridge link the MAI and PbI$_2$.[61] Similar results were also observed in our previous work. A stable transparent gel complex was obtained after the antisolvent extraction for the precursor solution with DMSO+MACl additives, In contrast the complex with only the MACl additive was not stable, transforming easily into a solid precipitate and losing fluidity after shaking several times (see the inset in Figure 8b).[19a] The XRD patterns at low angles confirm the formation of intermediate phase in both complexes before annealing (see Figure 8b). After annealing, the enhanced crystallinity with strong preferred orientation of the perovskite crystal was obtained for the stable gel complex with additive of DMSO+MACl (see Figure 8c), suggesting that the

ADVANCED
SCIENCE NEWS

www.advancedsciencenews.com

NANO · MICRO
small

www.small-journal.com

Figure 7. a) Photos of MAPbI₃ on FTO glass before and after annealing at 65 °C for 1 min and at 100 °C for 2 min. b) FTIR spectrometer of DMSO (solution), PbI₂·DMSO (powder), MAI·PbI₂·DMSO (powder). a,b) Reproduced with permission.[13c] Copyright 2015, American Chemical Society. c) Schematic illustrating the relation between the amount of DMSO and the component of intermediate film. Reproduced with permission.[38a] Copyright 2017, Elsevier Ltd.

stability of coordination complexes in perovskite precursor solution is correlated with the crystallinity of the final perovskite crystals.

The fabrication of perovskite thin films by the antisolvent assisted spin coating method is similar to the extraction of solvate from the perovskite precursor solution case discussed
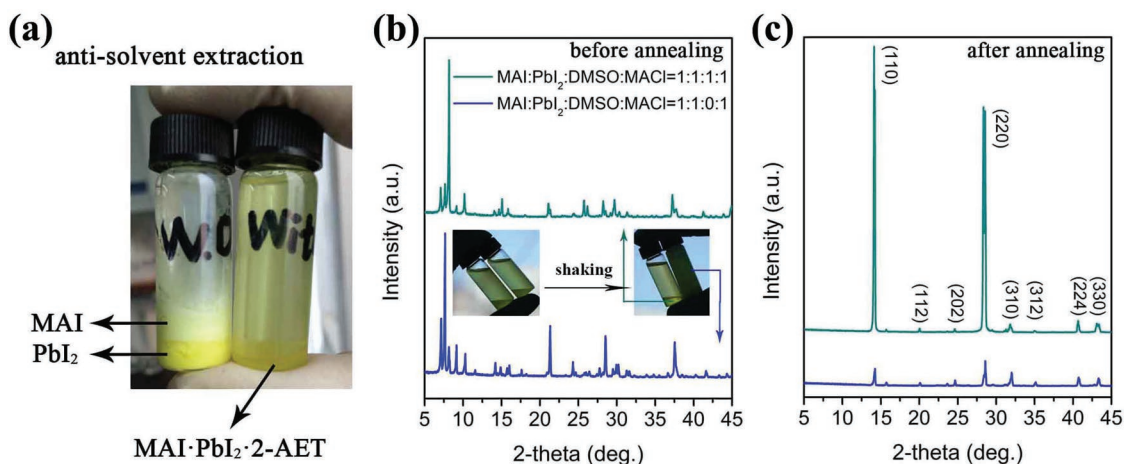
Figure 8. a) Photographs of perovskite precursor solutions extracted with ethyl acetate; in situ XRD patterns of the gel complexes extracted from colloidal perovskite precursors with MACl and DMSO+MACl additives, respectively, before annealing b) and after annealing c), the insets to (b) are photographs of the colloidal perovskite precursor solution extracted with ethyl acetate before and after shaking several times. Reproduced with permission.[19a] Copyright 2017, The Royal Society of Chemistry.

ADVANCED
SCIENCE NEWS
www.advancedsciencenews.com

NANO · MICRO
small
www.small-journal.com
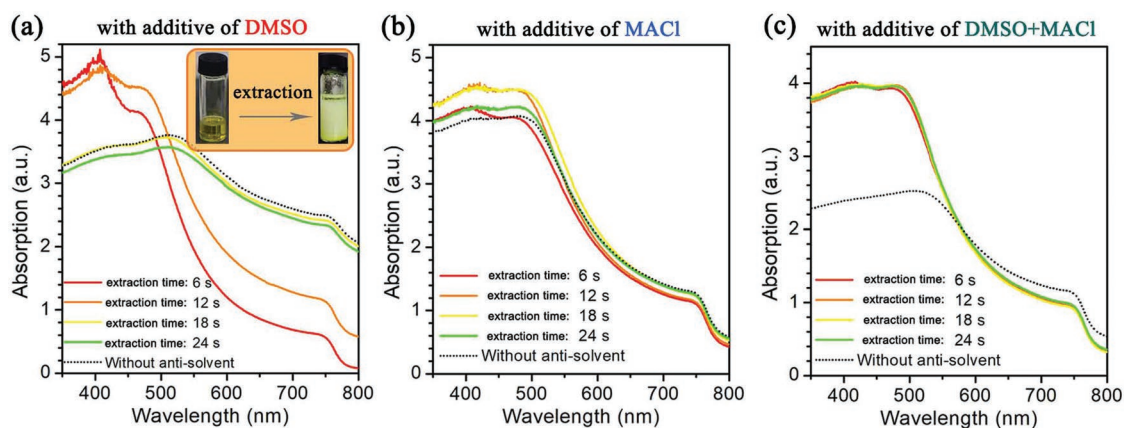
Figure 9. UV–vis absorption spectra of perovskite thin film prepared from different colloidal perovskite precursor with different antisolvent dipping time. a) DMSO added, with an inset showing photographs of the perovskite precursor before and after extraction by ethyl acetate; b) MACl added; c) DMSO+MACl added. Reproduced with permission.[19a] Copyright 2017, The Royal Society of Chemistry.

above in that the solvent is abruptly extracted from precursor wet films during the spin-coating. The stability of the obtained coordination complexes will thus also be one of the key factors to affect reproducibility. We found that due to the weak coordination interaction among MAI, PbI$_2$, and DMSO, the quality of the perovskite thin films exhibits a strong antisolvent dripping time dependence as shown in **Figure 9**a.[19a] The antisolvent processing windows for the perovskite precursor solution with MACl additive was enlarged to 18 s (see Figure 9b), which is attributed to the presence of a relatively stable gel coordination complex in the precursor solution with MACl additive. In the case of the perovskite precursor solution with DMSO+MACl additives, the presence of much more stable coordination complex in the precursor solution enhanced the reproducibility as expected, and the perovskite thin films no longer showed the antisolvent dripping time dependence and the operating windows was expanded over 24 s (see Figure 9c). A recent study revealed that there were hexagonal δ-phase, hexagonal polytypes, MAI-PbI$_2$-DMSO intermediate phases, and α-phase formed sequentially with different mixed-perovskite crystallization stages.[59e] Only the hexagonal δ-phase and MAI-PbI$_2$-DMSO intermediate phases readily converted to perovskite phase, while thermally stable hexagonal polytypes remained in the annealed films and deteriorated the device performance. This consists with the results above that the stability of intermediate phases should be responsible for the time sensitivity of fabricating perovskite thin films.

To avoid compromising the performance of the final perovskite thin films caused by the doping effect, the additives in the intermediate phase should be completely removed. In general, additives can be driven out from the intermediate phase adducts through volatilization, solvent extraction, or thermal annealing, depending on the boiling point and coordination ability of the additive. In the case of the additives with low boiling point and high volatility, the removal of additives could be triggered during the initial solidification process. For example, because of the facile removal of methylammonium acetate (MAAc) (see **Figure 10**a), the accelerated perovskite crystallization kinetics during the spin coating process was induced, which improved the perovskite morphology.[62] A similar strategy has been

reported to result in compact and smooth perovskite thin films by employing volatile NH$_4$Cl.[63] Besides, during the antisolvent extraction process, the additive could be driven out from the intermediate phase together with the solvent. For instance, transparent wet thin films of the MAI·PbI$_2$·DMSO intermediate phase were commonly observed after antisolvent treatment by diethyl ether,[13c] while there was a negligible amount of residual DMSO in the unannealed perovskite thin films by using the ethyl acetate as antisolvent.[64] This implies that the effect of the extraction ability of antisolvents on the removal of additive should be not ignored; further study of the influence of perovskite crystallization kinetics would provide more insights to improve the quality of perovskite thin films. Although perovskite crystallization can be significantly suppressed by incorporation of additives with strong coordination ability, the additives are hard to fully remove resulting in phase impurity. In our previous study,[16a] as shown in Figure 10b, residual thiourea was observed on the surface of the final perovskite thin films due to the strong coordination interaction between thiourea and PbI$_2$, which would increase interface charge recombination. Considering that the volatilization of thiourea from the coordination complex intermediate phase starts from a relatively high temperature of 175.4 °C,[16a] we developed a two antisolvent interfacial processing method to completely extract the residual thiourea from the surface and grain boundaries of the film at room temperature (see Figure 10c).

As illustrated in Figure 10d, the morphology evolution of perovskite with the residence time of additives can be summarized as follows. Volatile additives, such as MAAc and NH$_4$Cl, are driven out from the wet intermediate phase thin films during the spin coating process (before or with the evaporation of solvent), resulting in a high nucleation density and low crystal growth rate, so that smooth and compact perovskite thin films with small grain sizes (<200 nm) are obtained. Such films increase the charge recombination velocity that is deleterious to the transport and collection of charge carriers.[65] However, after the removal additives (such as DMSO) followed by the evaporation of solvents, the residual additives in the intermediate phases tend to reduce the nucleation density, which facilitates larger perovskite grains on the submicron scale. Since
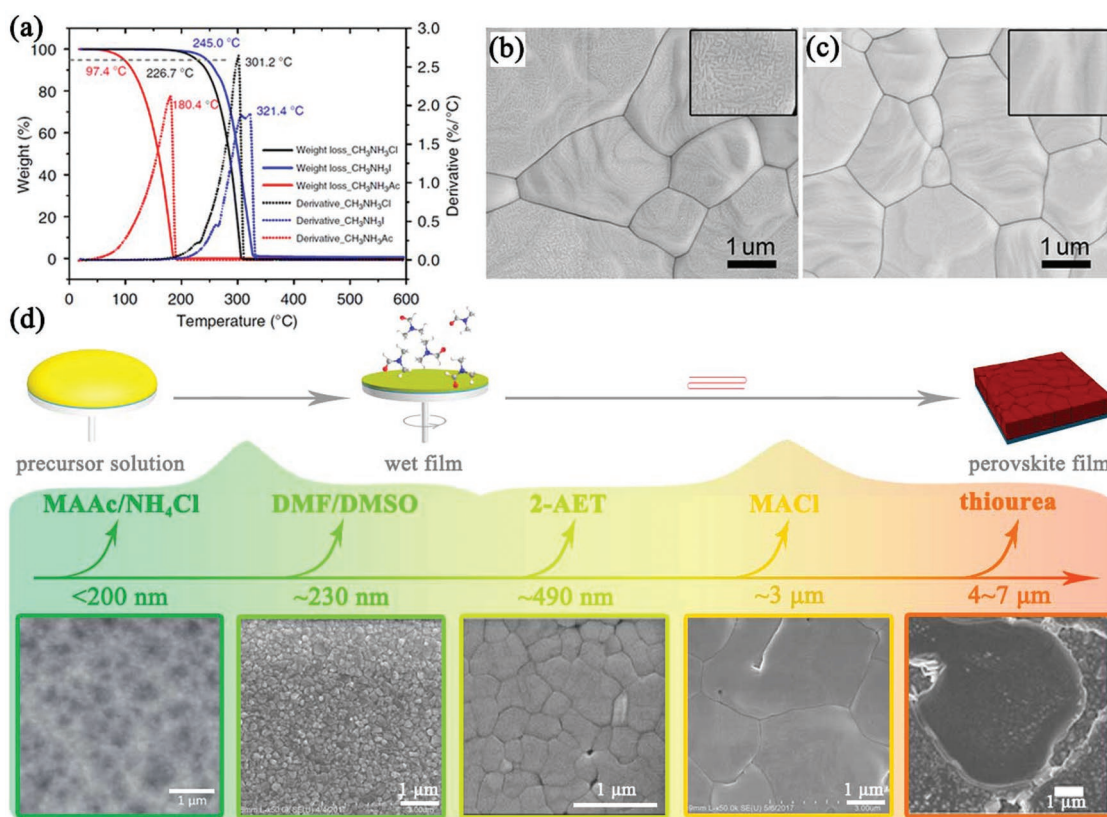
Figure 10. a) TGA curves and their derivatives for CH$_3$NH$_3$X (X = Cl, I, and Ac) in nitrogen atmosphere. Reproduced with permission.[66] Copyright 2015, Nature Publishing Group. SEM images of perovskite thin films prepared from different conditions: b) with thiourea-containing perovskite precursor, c) with thiourea-containing perovskite precursor and EA post-processing. Reproduced with permission.[16a] Copyright 2016, WILEY-VCH. d) Schematic illustration of the possible morphology evolution of perovskite with the residence time of additives in the intermediate phase.

the maximum growth rate of perovskite crystals is reached at higher temperature, a larger size of perovskite crystalline domains could be expected when the additives are removed during the annealing step.

Figure 11a,b illustrates the additive induced growth behavior of perovskite crystal mentioned above. During annealing, the morphology of the perovskite continues to evolve and the additives are gradually driven to the grain boundaries, which would increase the surface and interface energy and contribute to the thermodynamic driving force on the growth of the perovskite crystal. The process is analogous to the so-called solvent annealing strategy,[67] in which the activation energy of grain boundary migration would be reduced upon exposure to the solvent atmosphere, leading to the formation of larger perovskite grains. As a consequence, the amount of small perovskite grains tends to gradually reduce, and the compact perovskite thin films are formed with enlarged crystalline grains, with the longer the residence time of the additives, the larger the grain size.[61]

There is increasing consensus that although classic nucleation and growth theories provide a basic understanding of the growth of perovskite from the precursor solution, the grain size in the thin films is only weakly related to the degree of supersaturation. It implies that the growth of perovskite crystals may deviate from thermodynamic equilibrium. For example, the incorporation of an additive could change the structure of coordination complexes in the precursor solution and suppressed crystallization should be expected until full removal of the additives, secondary nucleation is possible and extra crystal growth is favored to minimize the energy of the surface and interfaces.

Nonclassical growth theories, such as Volmer–Weber growth (island growth) behavior,[68] Ostwald ripening,[69] and oriented-attachment[45a] have been used to try to describe the growth mechanism of perovskite crystals. Briefly, in Volmer–Weber growth, the precursor species favors mutual binding rather than binding to the substrate, the small clusters that do nucleate on the substrates surface form central nucleation sites, then islands initially coalesce from the pre-existed nuclei until the growth is interrupted by a neighboring island. However, Volmer–Weber growth behavior is only expected at a higher casted temperatures (>70 °C). In addition, much smaller perovskite grains appeared locally around the large ones, which have been attributed to the presence of nuclei inside the soft colloidal framework of precursor solution.[68] Ostwald ripening is related to thermodynamic disequilibrium, in which the total energy of the system can be decreased by increasing average grain size.[69,70] This behavior has been demonstrated for a perovskite film treated by a low-concentration of MABr, and requires small grains with higher surface energy in order to induce Ostwald ripening.[69] In the case of oriented-attachment theory, a single domain can be self-assembled by joining small particles at a
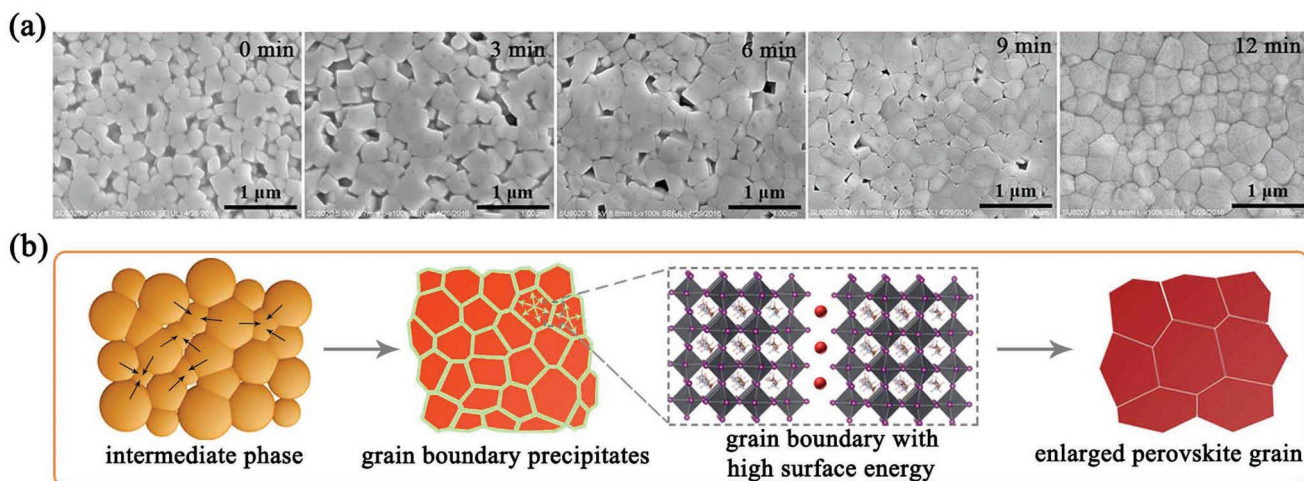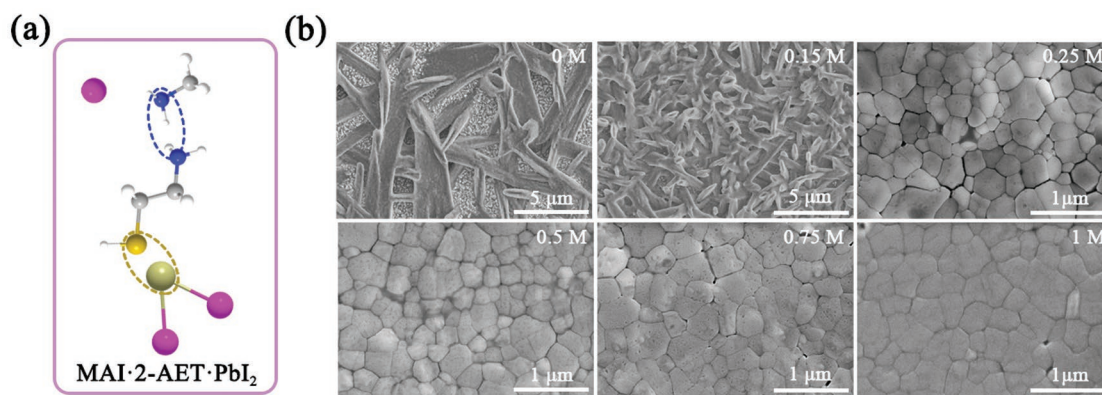
Figure 11. a) SEM images of MAPbI$_3$·(0.5)2-AET perovskite thin films with different annealing periods at 100 °C. Reproduced with permission.[61] Copyright 2016, The Royal Society of Chemistry. b) Schematic illustration of the morphology evolution of perovskite grains from intermediate phase films to perovskite thin films.

planar interface, which shares a common crystallographic orientation to minimize the surface free energy.[71] Despite the absence of strong evidence to suggest that particles agglomerates exist within the precursor prior to film formation,[45a] the oriented-attachment growth behavior is consistent with the results that the presence of defects, such as misfit dislocations, twin structures, and super-lattices are formed at the interface.[21,45a,72] In addition, Hu et al. proposed the following nanoassemble model of the formation of perovskite polycrystalline thin films from precursor solutions that contains Pb(Ac)$_2$ and MAI: 1) formation of solvate intermediate phase 1: the stable Pb-centered ion-cage (MAI)$_x$-PbI$_2$-(DMF)$_y$ is formed on removal of the solvent, which is stable at room temperature and commonly reported in the literatures; 2) conversion to intermediate phase 2: when the solvent is further removed, the solvate intermediate phase (MAI)$_x$-PbI$_2$-(DMF)$_y$ are forced into contact and transform into more stable perovskite crystals with PbI$_2$, MAI and another intermediate phase 2 (MAI)$_m$-PbI$_2$-(DMF)$_n$, which should be centered with a [PbI$_6$]$^{4-}$ octahedron and coordinated with MAI and DMF shells; 3) formation of perovskite: the solvate intermediate phase (MAI)$_x$-PbI$_2$-(DMF)$_y$ undergo

rapid decomposition at elevated temperature, leading to the formation of perovskite crystals, in this case, the emergence of intermediate (MAI)$_x$-PbI$_2$-(DMF)$_y$ is suppressed.[28b]
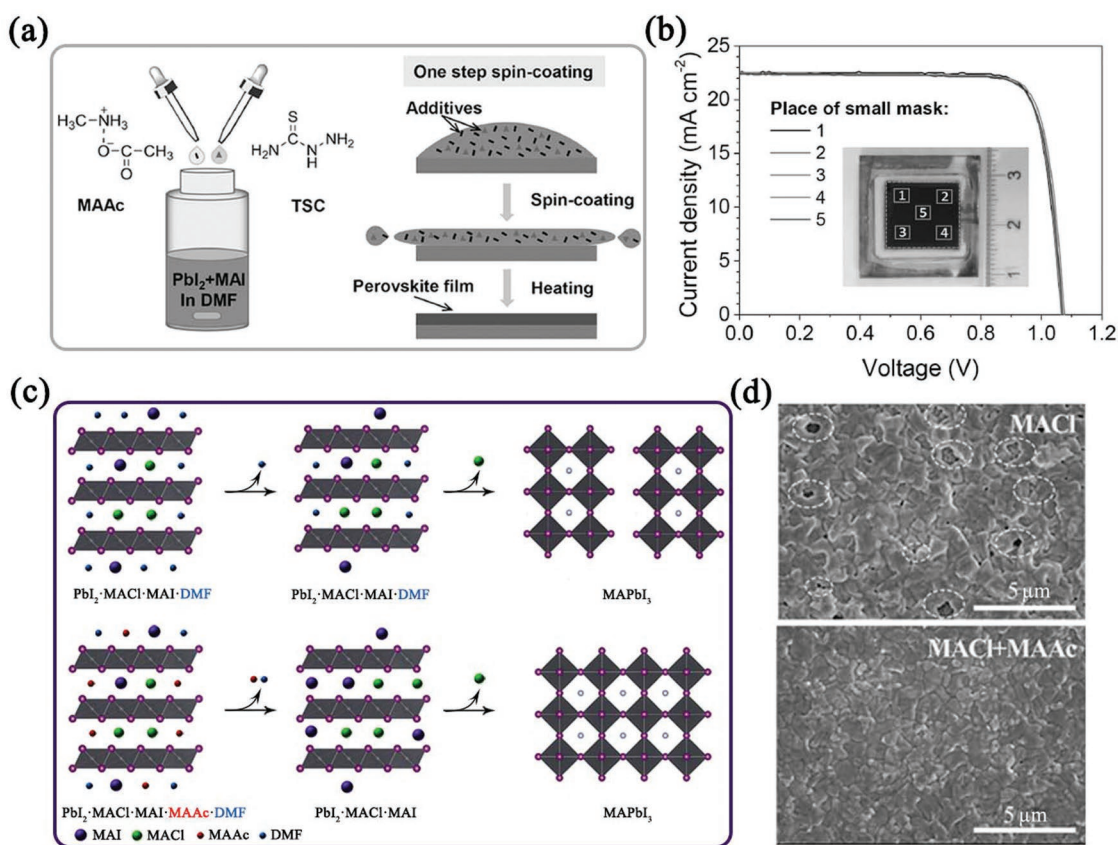
3.4. Antisolvent Free Strategy

So far, the best performing perovskite solar cells are fabricated by the antisolvent assisted spin-coating method.[12c,73] However, the limited cell size currently achievable by this method means that it is not well-suited to scalable industrial production.[49a,52a,74] Therefore, efforts in the design and development of an antisolvent free strategy are needed to meet the requirements of existing scalable fabrication methods. A chemical link between PbI$_2$ and MAI would avoid the asynchronous precipitation of the inorganic and organic components. As depicted in **Figure 12**a, we employed 2-AET as such a link. The stable MAI·PbI$_2$·2-AET coordination complex so formed eliminates the preferential growth of PbI$_2$, leading to homogeneous nucleation and growth environments for perovskite crystallization and, as a consequence, compact perovskite thin

Figure 12. a) Schematic illustration of the coordination interaction between MAI, PbI$_2$, and 2-AET; b) SEM images of MAPbI$_3$·(x)2-AET perovskite thin films prepared on FTO substrates, x = 0, 0.15, 1.25, 0.5, 0.75, and 1. Reproduced with permission.[61] Copyright 2016, The Royal Society of Chemistry.

**ADVANCED
SCIENCE NEWS**

www.advancedsciencenews.com
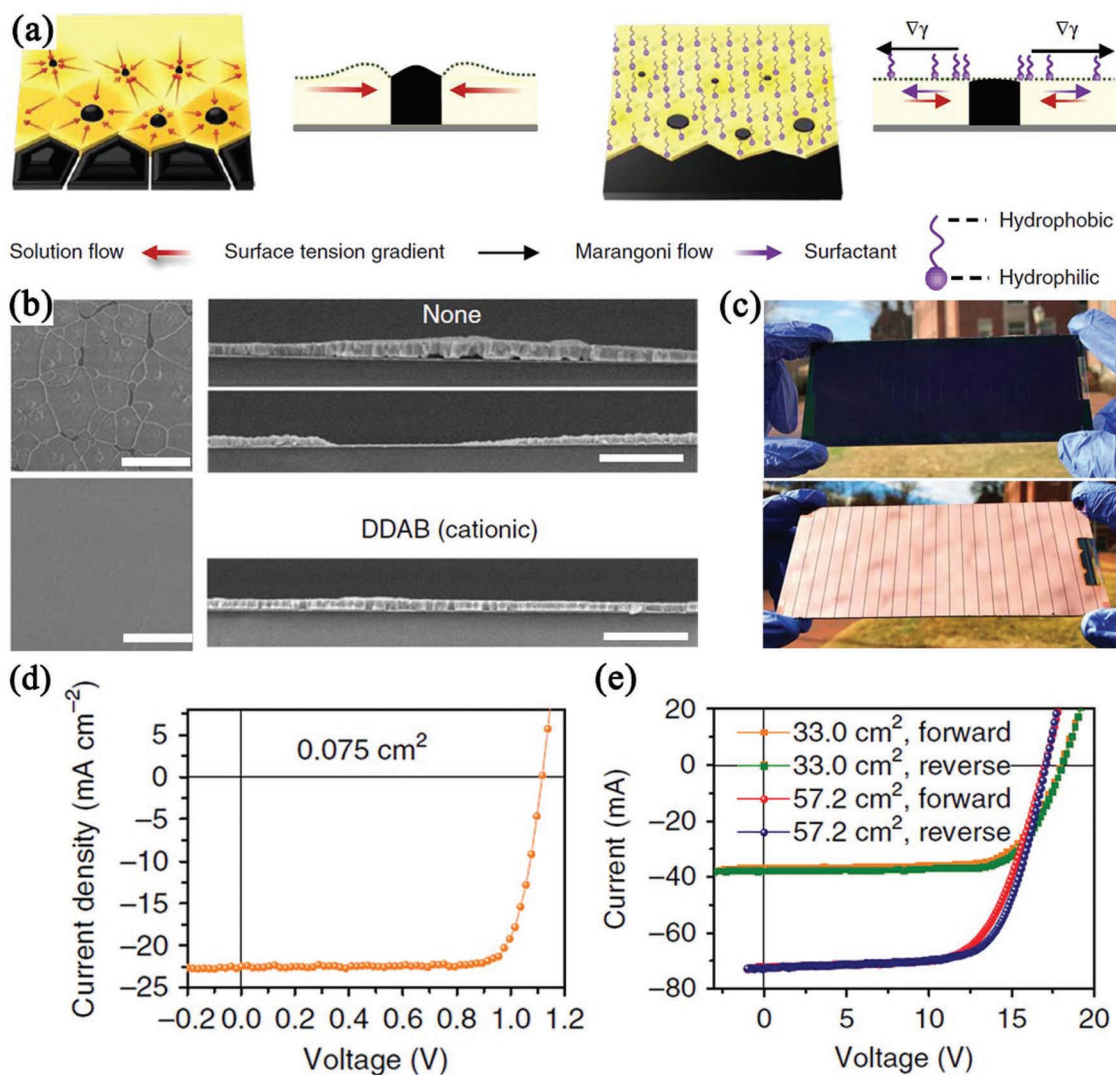
NANO · MICRO

small

www.small-journal.com

Figure 13. a) Schematic diagram of the additive-assisted one-step deposition of perovskite thin films, without any auxiliary operations like antisolvent dripping or vacuum. b) J–V curves measured from five different spots with an aperture area of 0.09 cm² selected from the large area device (active area of 1.21 cm²) as shown by the inset picture. a,b) Reproduced with permission.[17a] Copyright 2017, WILEY-VCH. c) Schematic illustration of the formation of a perovskite thin film from precursors with the MACl additive and the mixed additive of MACl+MAAc. d) Top-view SEM images of the perovskite thin films prepared by the antisolvent-free process using additives of MACl and MACl+MAAc. c,d) Reproduced with permission.[76] Copyright 2018, The Royal Society of Chemistry.

films with equiaxed grains were obtained after annealing (see Figure 12b).[61]

Recently, as shown in **Figure 13**a, Han and co-workers reported the synergetic additive strategy by employing several functional additives in perovskite precursor solution, in which the incorporation of MAAc in the solution increased the nucleation rate and improved the coverage of thin films, and a tiny amount of thio-semicarbazide additive significantly increased the perovskite grain size. This enables convenient fabrication of high-quality perovskite thin films with large crystals and low density of defects.[17a] The highest PCE obtained was over 19%, and the value of J_{sc} shows very small variation for the small cells at different positions located in a large size device (see Figure 13b). In addition, we studied the role of selected additives for an antisolvent free strategy by a combination of MACl and MAAc in the perovskite precursor solution.[75] As depicted in Figure 13c, the incorporation of MAAc with the MACl additive changes the composition of the coordination complexes. Ac⁻ has stronger coordination ability than DMF and so is able to occupy PbI_2 coordination sites can by partially displacing DMF molecules. During the drying process, the fast evaporation of MAAc from the precursor solution increases the nucleation rate and nuclei density of intermediate phase.

Subsequently, benefiting from the effect of MACl additive, larger perovskite grain sizes could be obtained after annealing (see Figure 13d).

To meet the requirement of industrially scalable deposition techniques, Huang and co-workers reported composition engineering by mixing Cs⁺ cation, Br⁻ anion and MACl into perovskite precursor solution, which enabled doctor blading coating of perovskite thin films at a lower temperature of 120 °C. Pinhole-free and smooth perovskite films with improved phase purity were readily obtained, yielding an improved stabilized PCE of 19.3%.[76] Later, they found that microscale particles of intermediate phase fluid moved toward perovskite islands during the drying of the perovskite ink after blading, so partially filled or empty gaps between the islands were formed.[77] They believed this phenomenon should be driven by the evaporation of solvents at the periphery of the perovskite islands (see **Figure 14**a). So the tiny amount (at the level of ≈20 parts per million) of surfactant additive in perovskite precursor solution was demonstrated to change the solution flow dynamics, as well as the adhesion of precursor solution to the substrates. This strategy enables blading of smooth perovskite films with an impressive coating rate of 180 m h⁻¹ (see Figure 14b,c), resulting in PCE of 20% for the small-area PSCs (0.075 cm²)

**ADVANCED
SCIENCE NEWS**

www.advancedsciencenews.com

NANO · MICRO

small

www.small-journal.com

Figure 14. a) Schematic illustration for the directional microscale solution flow toward perovskite island during ink drying; b) Plane view and cross-sectional SEM images of blade coated perovskite films without surfactant and with DDAB, respectively. Scale bars for plane view and cross-sectional SEM images are 50 and 5 μm, respectively; c) Photographic image of a perovskite solar module viewed from the glass side and top electrode side; d) J–V scanning of a 0.075 cm² surfactant-assisted blade-coated PSC. e) I–V scanning curves of modules with aperture areas of 33.0 and 57.2 cm². Reproduced with permission.[78] Copyright 2018, Nature Publishing Group.

and 15.3% and 14.6% for modules with aperture area of 33.0 and 57.2 cm², respectively.

4. Colloidal Characteristics of Perovskite Precursor Solutions

### 4.1. Effect of Colloidal Cluster Size on the Properties of Perovskite Grains

In classic nucleation and growth theories, a clear boundary divides a crystal from its precursor solution, while the structure of colloidal clusters, consisting of tens to hundreds of atoms with extra stability, are widely observed in the synthesis of nanoscale materials.[78] As discussed in Section 2.1, the perovskite precursor solutions are colloidal dispersions on the mesoscale, the colloidal cluster has a soft colloidal framework which consists of several iodoplumbate coordination complexes with a size range of 10–1000 nm according to dynamic light scattering results.[20,26,79] We confirmed that the size of the colloidal clusters in perovskite precursor solution could be controlled by the additive choice.[19a] As shown in **Figure 15**a, in the case of both additive-free perovskite precursor and with only DMSO additive, the average colloidal clusters size is around 100 nm, while it increases to 353 and 503 nm with MACl and DMSO+MACl additives, respectively. This suggests that the structure of colloidal clusters could be reconstructed by additives. However, the colloidal clusters are metastable and readily transform to perovskite as the solvent evaporated, making them hard to characterize. With the help of FTIR spectroscopy, we tracked the stretching vibration peak of the C=O bond of DMF to reveal the coordination interaction of colloidal clusters in the

ADVANCED
SCIENCE NEWS
www.advancedsciencenews.com

NANO · MICRO
small
www.small-journal.com
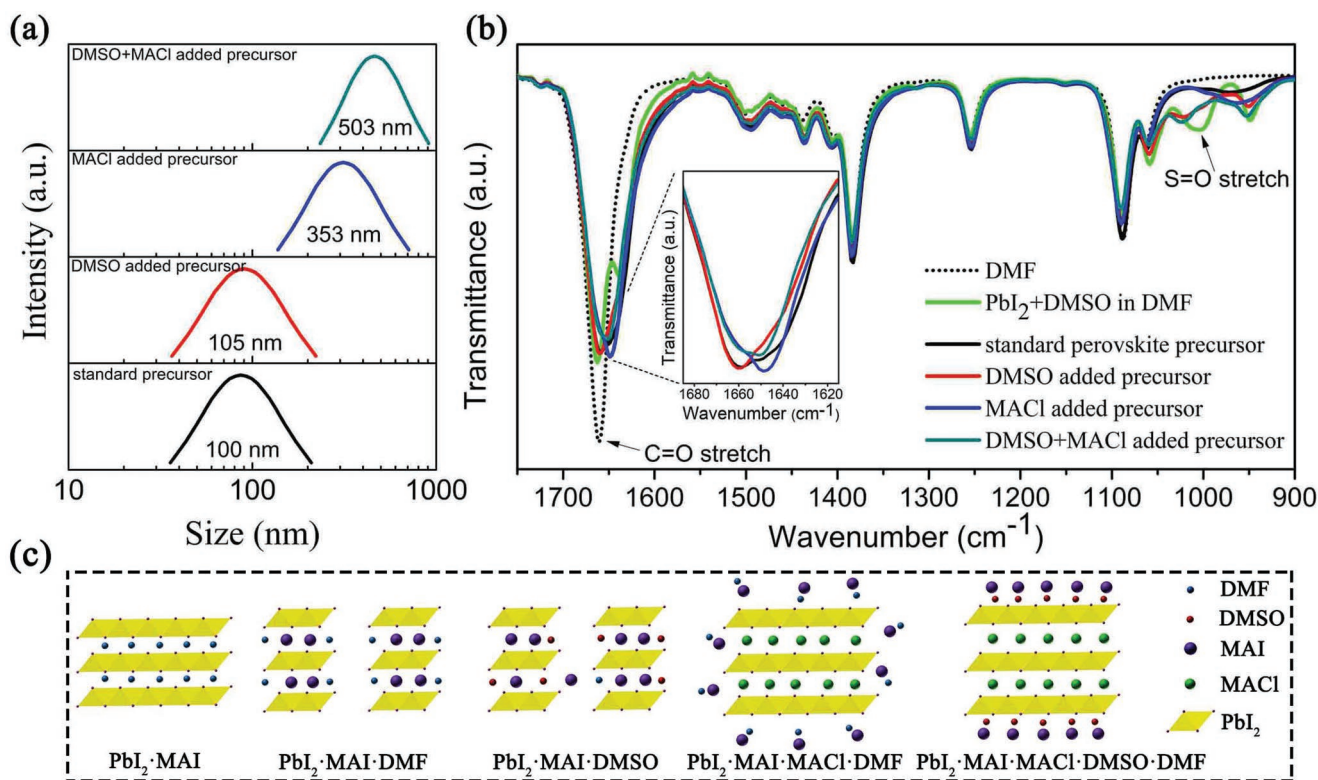
Figure 15. a) Size distributions of different colloidal perovskite precursors measured by DLS spectra; b) FTIR spectra of different colloidal perovskite precursors (inset: FTIR spectra of different colloidal perovskite precursors in the range of 1685–1615 cm⁻¹); c) Schematic illustration of the structure of colloidal clusters in different precursor solutions. Reproduced with permission.[19a] Copyright 2017, The Royal Society of Chemistry.

precursor solution (see Figure 15b). FTIR spectra show that the stretching vibration peak of the C=O bond of DMF appeared at 1660 cm⁻¹ for pure DMF, while it shifts to 1633 cm⁻¹ upon interacting with PbI₂. In the case of perovskite precursor solution, the stretching vibration peak of the C=O bond gets back to 1660 cm⁻¹, indicating the complexation between PbI₂ and I⁻ leads to the release of coordinated DMF molecules from Pb²⁺ centers. In addition, a small shoulder at 1650 cm⁻¹ is also identified, which is consistent with the frequency of that of MAI in DMF solution.[61] It implies that there is a coordinated MAI·DMF complex in the precursor solution, which leads to the exposure of the Pb²⁺ coordination center. Considering that the mole ratio of MAI:PbI₂ is 1:1 in the additive-free perovskite precursor solution, the result is consistent with the presence of some remaining PbI₂-DMF coordination, as indicated by the X-ray absorption near edge structure data discussed in Section 2.1. In the spectra taken from the perovskite precursor with MACl additive, the vibration peak of C=O shifts from 1660 to 1648 cm⁻¹, which is close to that of MAI·DMF complex as discussed above. Clearly, the affinity of coordination molecules toward PbI₂ is in order of DMF < DMSO < MAI < MACl, so we propose a possible substitution reaction that take place in perovskite precursor solution with MACl additive as in Equation (3)

$$MAI \cdot PbI_2 \cdot DMF + xMACl \rightarrow MAI_{1-x} \cdot PbI_2 \cdot MACl_x + (x)MAI \cdot DMF \quad (3)$$
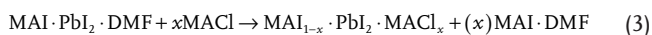
Based on this principle, and as depicted in Figure 15c, the MAI·PbI₂·DMF coordination complex in the normal

perovskite precursor solution transforms to $MAI_{1-x} \cdot PbI_2 \cdot$ additive$_x$ +(x)MAI·DMF upon interacting with the additives with stronger coordination ability than that of I⁻ toward PbI₂. We believe that such a substitution reaction is generally applicable and will be especially crucial to the principle of additive choice.

As revealed in **Figure 16**a,b, we found that a small size of colloidal clusters in the precursor solution produces a multilayer perovskite thin film with an average grain size of 230 nm. In contrast, monolayer-like perovskite thin films with micrometer-size crystalline grains can be obtained by using precursor solution with large colloidal clusters. Recently, Mitzi and co-workers reported an additive engineering approach to fabricating high-quality perovskite thin films at room temperature, employing methylammonium thiocyanate (MASCN) to control the perovskite crystallization.[16b] This work also highlights that the average grain size in perovskite thin films strongly correlates with colloidal clusters in precursor solution (see Figure 16c, d). Figure 16e summarizes the formation of perovskite thin films from colloidal perovskite precursor solutions; in particular, it shows the strong dependence of film morphology on colloidal cluster size.[19a] During film deposition, the sol precursor solutions alter into gel wet thin films after the removal of solvents. In the case of a small size of colloidal clusters (much less than the thickness of the wet thin film), a multilayer gel wet thin film is formed by close packing of small crystal grains. In contrast, large size colloidal clusters can be orderly arranged on the substrate to form monolayer-like gel wet films.

ADVANCED
SCIENCE NEWS
www.advancedsciencenews.com

NANO · MICRO
small
www.small-journal.com
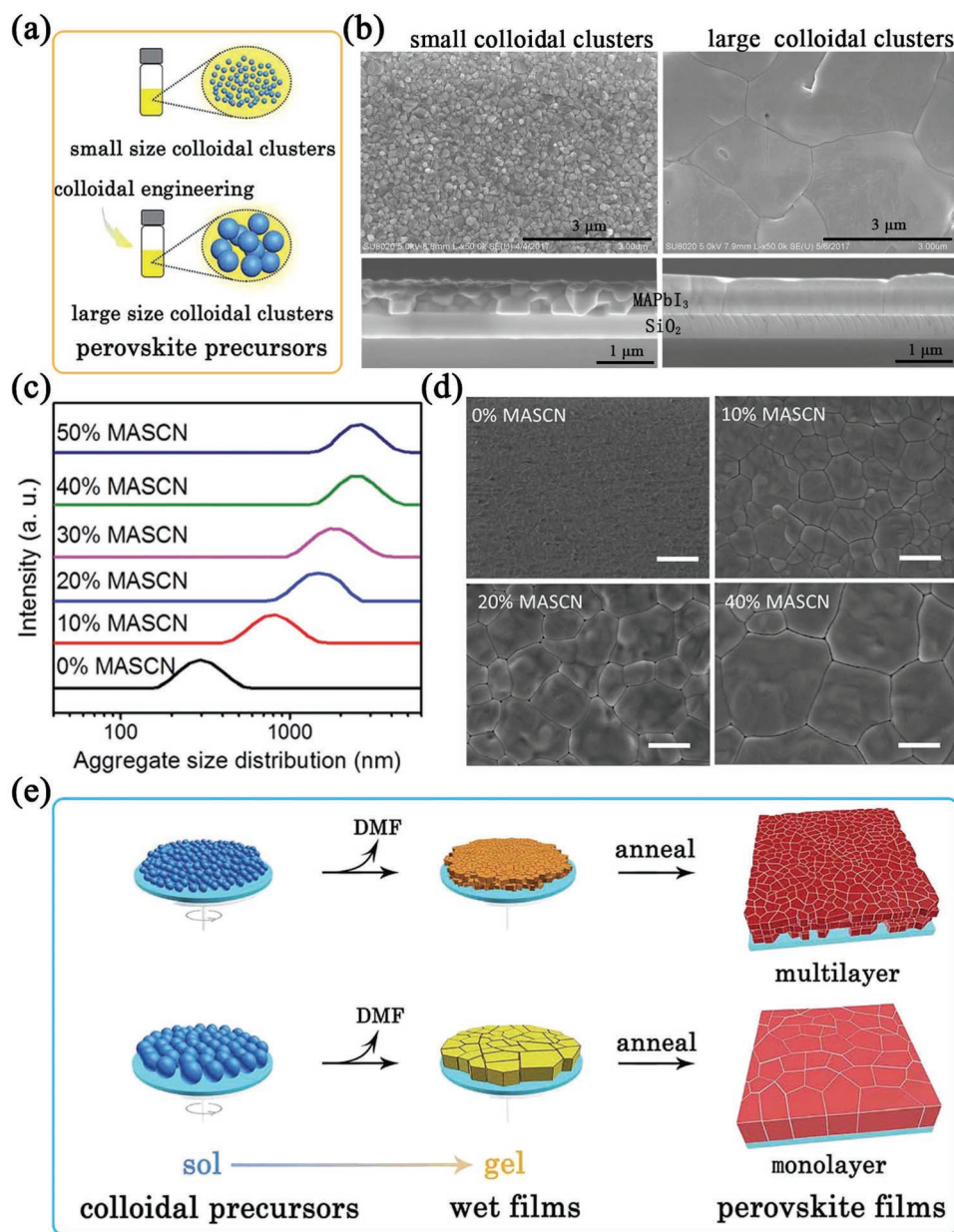
Figure 16. a) Schematic illustrations of the perovskite precursor solution with different size of colloidal clusters; b) Surface and cross-sectional SEM images of the perovskite thin films prepared using the precursors with different sizes of colloidal clusters. c) DLS data of MAPbI$_3$ precursor solutions with addition of an extra 5% PbI$_2$ and 0–50% MASCN. d) Top view SEM images of RT-MAPbI$_3$ films with addition of 5% extra PbI$_2$ and 0–50% MASCN to the precursor. The scale bar for the SEM images is 1 μm. c,d) Reproduced with permission.[16b] Copyright 2017, The Royal Society of Chemistry. e) Schematic illustrations of the formation process of perovskite thin films from colloidal precursors. b,e) Reproduced with permission.[19a] Copyright 2017, The Royal Society of Chemistry.

Then the intermediate phases of wet films transform into the perovskite structure during annealing, and nonclassical growth may dominate resulting in enlarged grain size.

4.2. Aging of Perovskite Precursor Solutions

Due to the chemical equilibrium between iodoplumbate coordination complexes and the competition among I$^-$, solvent molecules, and additive to interact with Pb^{2+}, the nature of perovskite

precursor solution is sensitive to the temperature,[36,80] components,[40,81] and aging.[82] In general, heating the precursor solution for extended duration at a mild temperature (70–180 °C) is suggested to fully dissolve the perovskite salts.[73a] A very recent study showed that separated perovskite precursor salts could not be fully dissolved in DMF within 2 h of aging. The accelerating dissolution of perovskite precursor salts should be expected due to the presence of complexation between PbI$_2$ and I$^-$ in precursor solution.[83] However, it is reported that the size of colloids clusters in perovskite precursor solution prepared

in GBL decreased with the increase of temperature due to the release of free ions into the solutions, leading to the shift of the equilibrium of the chemical reaction to the conversion of low-order iodoplumbates of Pb_3^- and PbI_2.[80] Nevertheless, the precursor solution aging time seems to become a critical factor in determining the size and structure of colloid clusters in the precursor solutions. Thus, it is important to establish a clear picture of the nucleation and growth processes of the colloidal clusters in the precursor solution and their correlation to the perovskite crystallization kinetics. Recently, inspired by the observation that colloid size increased from 190 nm to

above 500 nm when the precursor aging time reached 24 h, Tsai et al. depicted the perovskite precursor aging process by using a LaMer diagram.[82a] The formation of colloidal clusters in the precursor was described in the following steps: 1) Pre-nucleation: initial increase in the concentration of perovskite precursor salts without intermediates; 2) Burst-nucleation: fast nucleation of coordination complexes in the precursor solution; 3) Grown by diffusion: subsequent coordination complex growth via Ostwald ripening accompanied by a reduction of concentration in precursor solution. As shown in **Figure 17**a–d, there is an obvious increase in the perovskite grain size with
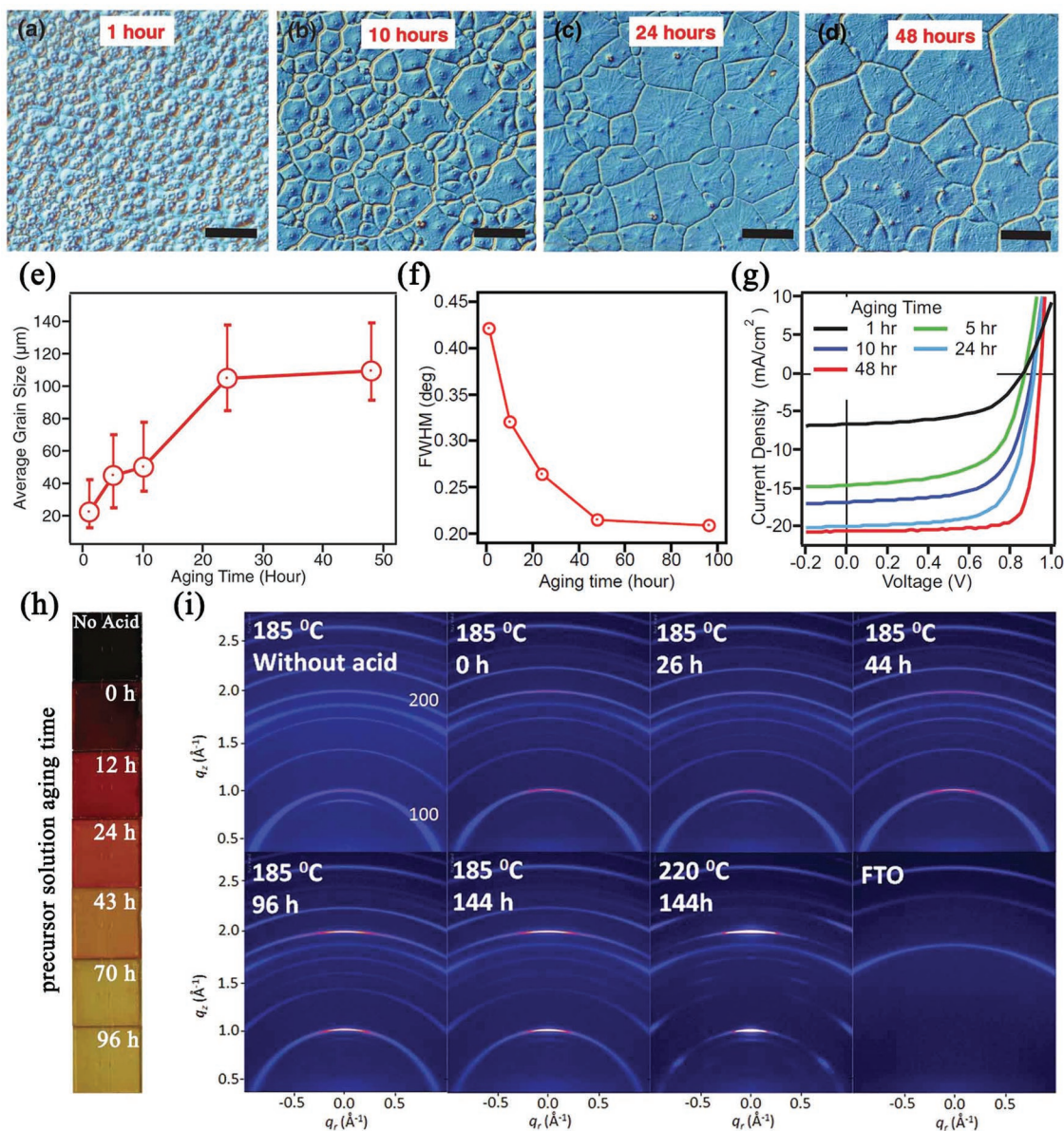
Figure 17. Optical microscope images of perovskite thin films produced by hot casting. The precursors are aged at different time points a) 1 h, b) 10 h, c) 24 h, and d) 48 h. The grain size varies from ≈20 to ≈110 µm (Scale bar: 50 µm); e) Average grain-size with error bar determined for 1–48 h aging time. f) Full width at half maximum (FWHM) of peaks of XRD patterns at $2\theta = 9.66°$ as a function of aging time. g) J–V characteristic curves of perovskite devices with different aging times. e–g) Reproduced with permission.[83a] Copyright 2017, WILEY-VCH. h) A series of photographs of thin films spin-coated and dried at 70 °C under nitrogen, prepared with solutions aged in an N_2 atmosphere for various periods of time after the addition of hydrohalic acid. i) A series of 2D X-ray diffraction patterns of corresponding thin film after full annealing step. h,i) Reproduced with permission.[83b] Copyright 2017, WILEY-VCH.

the perovskite precursor solution aging time. The average grain size dramatically increases from 20–50 to ≈105 µm within aging for 24 h, then tends to saturate to ≈110 µm (see Figure 17e). Benefiting from the enhanced crystallinity of perovskite thin films with the increase of precursor aging time, the average power conversion efficiency of perovskite solar cells improves from ≈2.5% to ≈15% (see Figure 17f,g). This suggests that it is beneficial to allow the growth of colloidal clusters in perovskite precursor solution for 1–2 days. The larger colloidal clusters in the precursor thus produced facilitate the fabrication of the high-quality perovskite thin films with enhanced crystallinity and optoelectronic properties. McMeekin et al. found that it took a period of tens to hundreds of hours for the gradual disappearance of the large size of colloid particles after the incorporation of additive hydriodic acid (HI) in the perovskite precursor solution.[82b] They proposed that the large colloidal clusters in the precursor would act as nucleation sites to initiate the formation of perovskite crystals. With increased aging time, the smaller colloidal clusters in the precursor solution tended to prolong the crystal conversion period due to fewer nucleation sites, which lead to the color change of the coated films (before annealing) from black to yellow as a function of precursor solution aging times (see Figure 17h). Furthermore, the significant texturing was observed for films prepared from the precursor solution due to the extended growth stage.

5. DMF/DMSO-Free Perovskite Precursor Solutions

To date, DMF or a mixture of DMF and DMSO are commonly used as the solvent for the perovskite precursor solutions involved in the fabrication of high efficient perovskite devices.[30a,42b,84] However, the toxicity of these solvents will limit their use in future large scale manufacturing. It is thus imperative to develop alternatives so as to protect personal safety and avoid environmental pollution.

In a recent study, Zhou et al. reported a reversible perovskite-gas interaction: upon exposure to methylamine (MA) gas, the perovskite crystals were observed to melt into the liquid intermediate phase of $MAPbI_3 \cdot (x)MA$.[85] After removal of the MA gas, reconstruction of high-quality perovskite occurred. This reaction was attributed to the coordination interaction between the Pb atom in PbI_6-octahedra framework and N atom in MA molecules. This solid–liquid reaction provides an important insight that the dissolution of PbI_2 crystal may be not limited to the commonly used organic solvents, which inspired the later discovery of the development the DMF/DMSO free perovskite precursor solution system.

Noel et al. reported a DMF-free perovskite precursor solution by employing the composite acetonitrile (ACN)/MA solvent system to fully dissolve the $MAPbI_3$ precursor salts.[32] As shown in **Figure 18**a, in the case of the perovskite precursor salts dissolved in ACN, a black precipitate of $MAPbI_3$ was formed due to the weak solvate power of ACN as discussed above, while a clear pale yellow perovskite precursor solution was obtained upon the addition of MA gas in ACN solvent. The introduction of the low boiling point solvent ACN in this approach also facilitates the rapid crystallization of perovskite
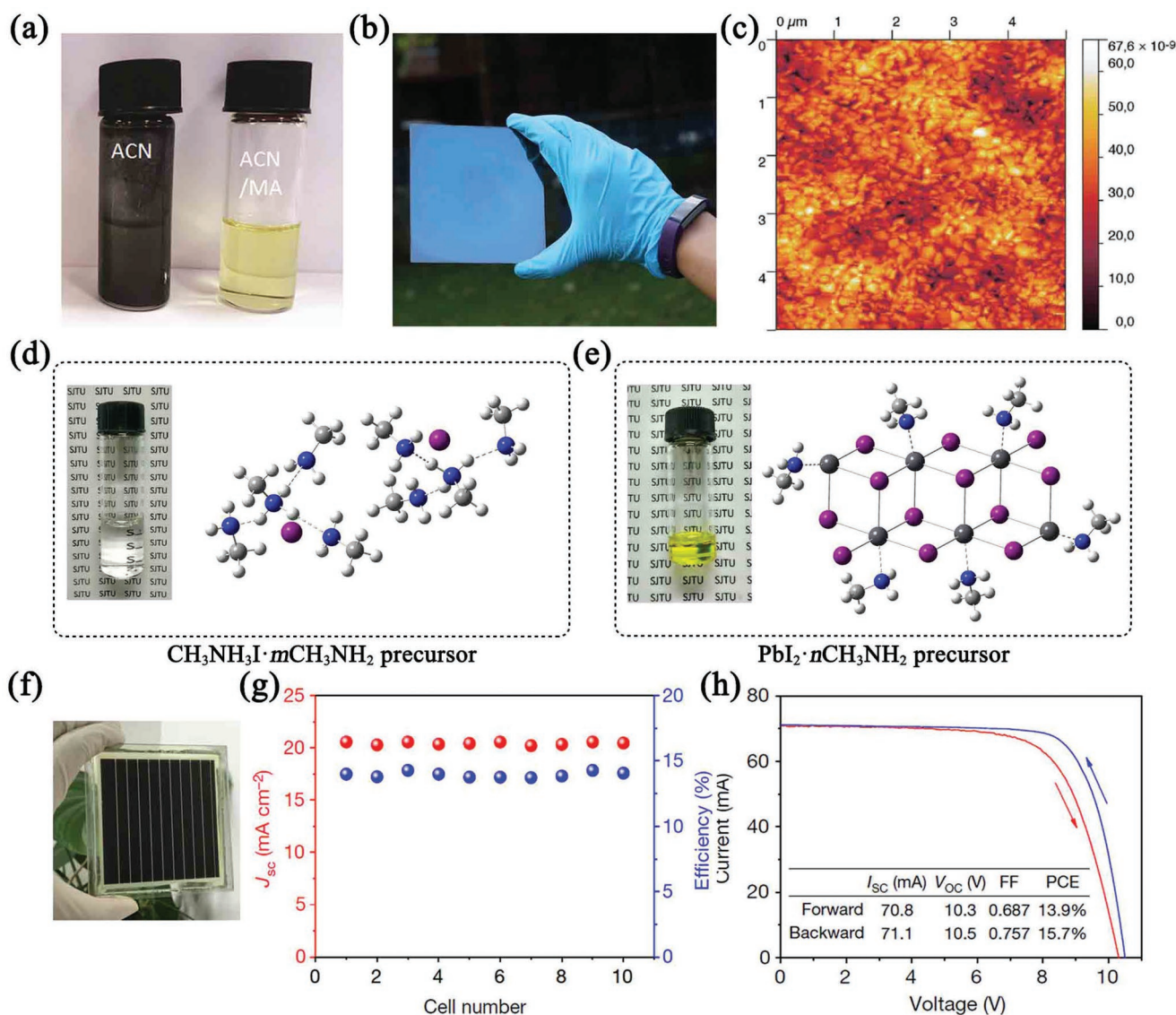
at room temperature, so that smooth, mirror-like, and uniform large areas (125 cm^2) perovskite thin film with a very small root mean square (rms) value of 7.8 nm was deposited from the ACN/MA solvent system (see Figure 18b,c). As depicted in Figure 18d,e, except for the Pb-N coordination interaction between PbI_2 and MA, the presence of molecular interactions between both perovskite precursor salts (MAX and PbX_2, X = I⁻, Br⁻, and Cl⁻) and MA gas have also been confirmed through the interaction between –NH₃⁺ and –NH₂ or Pb²⁺ and –NH₂.[86] The solid powder of MAI·mMA transformed to a clear liquid amine complex for m values up to 3, while the pale yellow paste of amine complex $PbI_2 \cdot MA$ was produced by the interaction between PbI_2 and MA gas (see Figure 18e). The clear yellow liquid state solvent-free perovskite precursor was obtained by directly mixing the two types of amine complex precursors in a mole ratio of 1:1. Due to the presence of the rapid conversion of amine precursors to perovskite thin films, a pressure processing method was developed to deposit highly uniform and pin-hole free large area perovskite thin films (64 cm^2). As shown in Figure 18f,g, the 10 sub-cells show good reproducibility from cell to cell, a PCE of 15.7% was obtained measured in the backward direction with illuminated aperture area of 36.1 cm^2. These methods open up a new route to the future scalable manufacture of high-quality perovskite thin films. Recently, Chao et al. demonstrated an environmentally room-temperature molten salt of MAAc as a solvent for facile fabrication of PSCs in ambient air. In comparison with DMF and DMSO, the low vapor pressure of MAAc allows the fabrication of a pin-hole free, smooth-surfaced, and high-quality perovskite thin films via a simple annealing-assisted solution process method, yielding of a PCE a 20.05% with excellent stability in air.[87]

6. Degradation of Perovskite Precursor Solutions

The short-term aging of perovskite precursor solutions up to several days has been demonstrated to improve the crystal quality and morphology of perovskite thin film. However, the long-term stability and shelf-life of the precursor solution also needs to be considered. For example, the black $MA_{0.17}FA_{0.83}Pb(I_{0.83}Br_{0.17})_3$ perovskite thin films can be obtained from freshly made precursor solutions (See **Figure 19**a).[88] However, the appearance of the thin films becomes visually lighter as the precursor solution is stored for a longer time (>12 days), accompanied with the gradual PL quenching and a decrease in device efficiency (See Figure 19b,c).[88,89]

Several possible mechanisms of precursor solution degradation have been investigated. For example, the hydrolysis of DMF solvent induced by trace water would result in the formation of formic acid (HCOOH) and dimethylammonium (DMA) on timescales of days to several weeks even in inert storage conditions (see Figure 19d), and DMA⁺ could incorporate into the perovskite crystal lattice to replace MA⁺ and Cs⁺.[89] As a result, the formation of nonstoichiometric perovskite thin films could deteriorate the optoelectronic properties of the final perovskite thin films and devices. Besides, there is increasing consensus that the color of perovskite precursor solution change from light yellow to dark brown due to the fact that I⁻ tends to be oxidized to form I_2 in the precursor solution (see Figure 19e).[20,30b] This

**ADVANCED
SCIENCE NEWS**

www.advancedsciencenews.com

NANO · MICRO

small

www.small-journal.com

Figure 18. a) Vials of perovskite precursors $CH_3NH_3I:PbI_2$ (1: 1.06 molar ratio) in neat ACN, and in the ACN/MA solvent mixture. b) Photographs of a 125 cm^2, highly specular, pinhole free film of $CH_3NH_3PbI_3$ deposited via spin coating from the ACN/MA solvent system. a,b) Reproduced with permission.[31] Copyright 2017, The Royal Society of Chemistry. c) A 5 $\mu m \times 5$ μm AFM image of the perovskite film shown in (b); schematic structure and appearance of the precursor $CH_3NH_3I \cdot mCH_3NH_2$ d) and $PbI_2 \cdot nCH_3NH_2$ e). Photograph of a module f) and the photocurrent density (J_{SC}) and efficiency of each sub-cell g). h) I–V curves of a solar module measured in backward (from V_{OC} to I_{SC}) and forward (from I_{SC} to V_{OC}) modes under simulated solar light, AM 1.5G, 100 mW cm^{-2}. c–h) Reproduced with permission.[87] Copyright 2017, Nature Publishing Group.

formation of I_2 may lead to an iodide deficiency in perovskite thin films, which is correlated with an increasing trap state density in perovskite thin films.[30b,90] Some progress has been made toward the elimination of the remnant I_2 in the oxidized precursor, with the addition of hypophosphorous acid (HPA) and MA in perovskite precursor solution reported to effectively suppress I_2 impurities.[20,90]

7. Conclusion and Outlook

There has been significant progress in just a few years in the fundamental understanding of perovskite precursor solution

chemistry leading to high-quality perovskite thin films with micron-sized grains, enhanced crystallinity, low defects density, and microsecond-range carrier lifetimes. In this Review, we have presented and discussed the nature of perovskite precursor solutions and tried to relate this understanding to the properties of the perovskite thin films fabricated from them. It is clear that perovskite precursor solutions are a mixture of various iodoplumbate coordination complexes in a polar aprotic organic solvent, and there are competitions among organic component, solvent, and additive to coordinate with PbI_2. Perovskite thin films are formed via heterogeneous nucleation accompanied by rapid solvent evaporation, followed by fast crystallization due to a low activation energy. The nucleation of
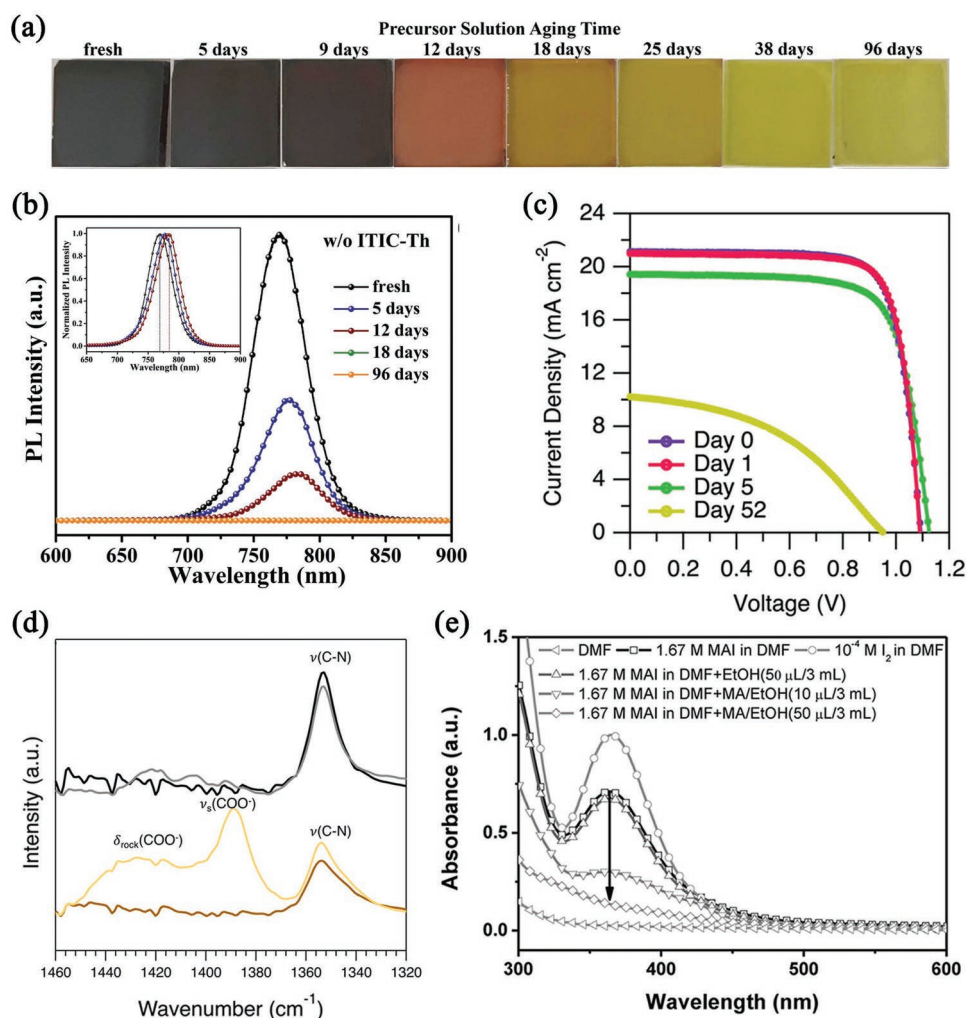
Figure 19. A series of photographs a) and steady-state PL spectra b) of films fabricated by perovskite precursor solutions aged for different amount of time. Reproduced with permission.[88] Copyright 2018, WILEY-VCH. c) Open-circuit voltage to short-circuit current scanned (reserve scan) J–V curves fabricated with FAMACs ink stored for different times: fresh ink and 1, 5, and 52 days. d) FTIR spectra of FAMACs films that are fabricated from fresh ink (black lines) and 240 days old ink (yellow lines). Lighter lines are before annealing, and darker lines are after annealing. c,d) Reproduced with permission.[89] Copyright 2018, American Chemical Society. e) UV–visible absorption spectra of MAI or I_2 dissolved in DMF and the corresponding absorbance spectra. Reproduced with permission.[20] Copyright 2017, WILEY-VCH.

the perovskite can be broadly explained by the classical theory, although there is no clear boundary dividing the perovskite intermediate phase from its precursor solution due to the presence of a series of self-assembled colloidal clusters. As expected, any shift of the equilibria would change the coordination complex species, as well as the crystallization kinetics. As a result, the subsequent growth of perovskite crystals may deviate from thermodynamic equilibrium. In particular, the increased energy of the surface and interface induced by additives or intermediate phases along the grain boundaries may drive secondary nucleation, and extra crystal growth is favored to minimize the energy.

To meet the requirements of future scalable fabrication of PSCs, development of the precursor solution is a key factor to achieve efficient and reproducible perovskite solar modules. In comparison with conventional spin-coating process, the solvent-drying process is challenging when enlarging the coating area, because the continuous and homogeneous perovskite thin films can be produced only by balancing the competition between the solvent evaporation rate, solute diffusion rate, and perovskite growth rate. In addition, to avoid the asynchronous precipitation of the inorganic and organic components caused by different solubility, the stability of coordination complexes in precursor solutions should be improved by chemical link, which would be expected to provide homogeneous nucleation and growth environments for perovskite.

Although investigations have already revealed the strong link between precursor solutions and the performance of perovskite thin films, further research is still required. The challenges that remain to be addressed in the future include:

1) The exact structure of the colloidal clusters in the perovskite precursor solution are still not known so that the underlying mechanism by which perovskite crystals form from the

ADVANCED
SCIENCE NEWS

www.advancedsciencenews.com

NANO · MICRO

small

www.small-journal.com

precursor solutions is not fully clear. Advanced characterization techniques are needed to directly investigate the exact structures of colloidal clusters.

2) Reliable correlations between the stoichiometric ratio of the perovskite salts in the precursor solutions and the properties of the final perovskite thin films need to be established.

3) The compositional segregation of organic component in intermediate phase. Additives with strong coordination ability can form stable coordination complexes of $PbI_2 \cdot$ additives, leading to the compositional segregation of organic component. The organic component can then react with free PbI_2 via solid phase diffusion to form perovskite until the additive molecules are driven out from the intermediate phase, which may cause the formation of both halide anion and organic cation vacancy defects due to the low solid phase diffusion rate. Chemical link between organic and inorganic components is expected to improve the stability of coordination complexes in precursor solutions, leading to the homogeneous nucleation and growth environments for perovskite.

4) The degradation of the perovskite precursor solution with aging. Developing stabilizer for precursor solution is necessary to improve the long-term stability of perovskite precursor solution.

5) To protect personal safety and avoid environmental pollution, nontoxic solvents without sacrifice the performance of perovskite thin films should be developed.

Conflict of Interest

The authors declare no conflict of interest.

[1] D. Weber, *Z. Naturforsch., B: J. Chem. Sci.* **1978**, *33*, 1443.

[2] a) H. S. Kim, C. R. Lee, J. H. Im, K. B. Lee, T. Moehl, A. Marchioro, S. J. Moon, R. Humphry-Baker, J. H. Yum, J. E. Moser, M. Gratzel, N. G. Park, *Sci. Rep.* **2012**, *2*, 591; b) O. Ergen, S. M. Gilbert, T. Pham, S. J. Turner, M. T. Z. Tan, M. A. Worsley, A. Zettl, *Nat. Mater.* **2017**, *16*, 522.

[3] a) V. D'Innocenzo, G. Grancini, M. J. Alcocer, A. R. Kandada, S. D. Stranks, M. M. Lee, G. Lanzani, H. J. Snaith, A. Petrozza, *Nat. Commun.* **2014**, *5*, 3586; b) M. Saba, M. Cadelano, D. Marongiu, F. Chen, V. Sarritzu, N. Sestu, C. Figus, M. Aresti, R. Piras,

[4] a) S. D. Stranks, G. E. Eperon, G. Grancini, C. Menelaou, M. J. Alcocer, T. Leijtens, L. M. Herz, A. Petrozza, H. J. Snaith, *Science* **2013**, *342*, 341; b) G. Xing, N. Mathews, S. Sun, S. S. Lim, Y. M. Lam, M. Gratzel, S. Mhaisalkar, T. C. Sum, *Science* **2013**, *342*, 344; c) Q. Dong, Y. Fang, Y. Shao, P. Mulligan, J. Qiu, L. Cao, J. Huang, *Science* **2015**, *347*, 967.

[5] a) W.-J. Yin, T. Shi, Y. Yan, *Appl. Phys. Lett.* **2014**, *104*, 063903; b) K. X. Steirer, P. Schulz, G. Teeter, V. Stevanovic, M. Yang, K. Zhu, J. J. Berry, *ACS Energy Lett.* **2016**, *1*, 360; c) R. E. Brandt, J. R. Poindexter, P. Gorai, R. C. Kurchin, R. L. Z. Hoye, L. Nienhaus, M. W. B. Wilson, J. A. Polizzotti, R. Sereika, R. Žaltauskas, L. C. Lee, J. L. MacManus-Driscoll, M. Bawendi, V. Stevanović, T. Buonassisi, *Chem. Mater.* **2017**, *29*, 4667; d) L. K. Ono, S. Liu, Y. Qi, *Angew. Chem., Int. Ed. Engl.* **2019**, https://doi.org/10.1002/anie.201905521.

[6] a) J. Huang, Y. Yuan, Y. Shao, Y. Yan, *Nat. Rev. Mater.* **2017**, *2*, 17042; b) D. T. Moore, H. Sai, K. W. Tan, D. M. Smilgies, W. Zhang, H. J. Snaith, U. Wiesner, L. A. Estroff, *J. Am. Chem. Soc.* **2015**, *137*, 2350.

[7] H. Miyasaka, Y. Satoh, Y. Ishibashi, S. Ito, Y. Nagasawa, S. Taniguchi, H. Chosrowjan, N. Mataga, D. Kato, A. Kikuchi, J. Abe, *J. Am. Chem. Soc.* **2009**, *131*, 7256.

[8] NREL, https://www.nrel.gov/pv/assets/images/efficiency-chart.png (accessed: August **2019**).

[9] N. J. Jeon, J. H. Noh, Y. C. Kim, W. S. Yang, S. Ryu, S. I. Seok, *Nat. Mater.* **2014**, *13*, 897.

[10] a) J. Burschka, N. Pellet, S. J. Moon, R. Humphry-Baker, P. Gao, M. K. Nazeeruddin, M. Gratzel, *Nature* **2013**, *499*, 316; b) J. H. Im, I. H. Jang, N. Pellet, M. Gratzel, N. G. Park, *Nat. Nanotechnol.* **2014**, *9*, 927.

[11] a) Y. Deng, E. Peng, Y. Shao, Z. Xiao, Q. Dong, J. Huang, *Energy Environ. Sci.* **2015**, *8*, 1544; b) W.-Q. Wu, Z. Yang, P. N. Rudd, Y. Shao, X. Dai, H. Wei, J. Zhao, Y. Fang, Q. Wang, Y. Liu, Y. Deng, X. Xiao, Y. Feng, J. Huang, *Sci. Adv.* **2019**, *5*, eaav8925.

[12] a) N. J. Jeon, J. H. Noh, W. S. Yang, Y. C. Kim, S. Ryu, J. Seo, S. I. Seok, *Nature* **2015**, *517*, 476; b) D. Bi, C. Yi, J. Luo, J.-D. Décoppet, F. Zhang, S. M. Zakeeruddin, X. Li, A. Hagfeldt, M. Grätzel, *Nat. Energy* **2016**, *1*, 16142; c) G. Zheng, C. Zhu, J. Ma, X. Zhang, G. Tang, R. Li, Y. Chen, L. Li, J. Hu, J. Hong, Q. Chen, X. Gao, H. Zhou, *Nat. Commun.* **2018**, *9*, 2793; d) E. H. Jung, N. J. Jeon, E. Y. Park, C. S. Moon, T. J. Shin, T.-Y. Yang, J. H. Noh, J. Seo, *Nature* **2019**, *567*, 511; e) N. J. Jeon, H. Na, E. H. Jung, T.-Y. Yang, Y. G. Lee, G. Kim, H.-W. Shin, S. Il Seok, J. Lee, J. Seo, *Nat. Energy* **2018**, *3*, 682; f) W. A. Dunlap-Shohl, Y. Zhou, N. P. Padture, D. B. Mitzi, *Chem. Rev.* **2019**, *119*, 3193.

[13] a) F. Huang, Y. Dkhissi, W. Huang, M. Xiao, I. Benesperi, S. Rubanov, Y. Zhu, X. Lin, L. Jiang, Y. Zhou, A. Gray-Weale, J. Etheridge, C. R. McNeill, R. A. Caruso, U. Bach, L. Spiccia, Y.-B. Cheng, *Nano Energy* **2014**, *10*, 10; b) M. Xiao, F. Huang, W. Huang, Y. Dkhissi, Y. Zhu, J. Etheridge, A. Gray-Weale, U. Bach, Y. B. Cheng, L. Spiccia, *Angew. Chem.* **2014**, *126*, 10056; c) N. Ahn, D. Y. Son, I. H. Jang, S. M. Kang, M. Choi, N. G. Park, *J. Am. Chem. Soc.* **2015**, *137*, 8696; d) S. Bae, S. J. Han, T. J. Shin, W. H. Jo, *J. Mater. Chem. A* **2015**, *3*, 23964.

[14] C. Fei, L. Guo, B. Li, R. Zhang, H. Fu, J. Tian, G. Cao, *Nano Energy* **2016**, *27*, 17.

[15] a) M. Yang, Z. Li, M. O. Reese, O. G. Reid, D. H. Kim, S. Siol, T. R. Klein, Y. Yan, J. J. Berry, M. F. A. M. van Hest, K. Zhu, *Nat. Energy* **2017**, *2*, 17038; b) R. A. Kerner, L. Zhao, Z. Xiao, B. P. Rand, *J. Mater. Chem. A* **2016**, *4*, 8308.

[16] a) C. Fei, B. Li, R. Zhang, H. Fu, J. Tian, G. Cao, *Adv. Energy Mater.* **2017**, *7*, 1602017; b) Q. Han, Y. Bai, J. Liu, K.-z. Du, T. Li, D. Ji, Y. Zhou, C. Cao, D. Shin, J. Ding, A. D. Franklin, J. T. Glass, J. Hu,

M. J. Therien, J. Liu, D. B. Mitzi, *Energy Environ. Sci.* **2017**, *10*, 2365; c) Y. Yu, C. Wang, C. R. Grice, N. Shrestha, D. Zhao, W. Liao, L. Guan, R. A. Awni, W. Meng, A. J. Cimaroli, K. Zhu, R. J. Ellingson, Y. Yan, *ACS Energy Lett.* **2017**, *2*, 1177; d) H.-C. Liao, P. Guo, C.-P. Hsu, M. Lin, B. Wang, L. Zeng, W. Huang, C. M. M. Soe, W.-F. Su, M. J. Bedzyk, M. R. Wasielewski, A. Facchetti, R. P. H. Chang, M. G. Kanatzidis, T. J. Marks, *Adv. Energy Mater.* **2017**, *7*, 1601660; e) Y. Zhang, Z. Fei, P. Gao, Y. Lee, F. F. Tirani, R. Scopelliti, Y. Feng, P. J. Dyson, M. K. Nazeeruddin, *Adv. Mater.* **2017**, *29*, 1702157; f) S. S. Mali, J. V. Patil, H. Kim, H. Kim, C. K. Hong, *Adv. Funct. Mater.* **2019**, *29*, 1807420.

[17] a) Y. Wu, F. Xie, H. Chen, X. Yang, H. Su, M. Cai, Z. Zhou, T. Noda, L. Han, *Adv. Mater.* **2017**, *29*, 1701073; b) Z. Huang, X. Hu, C. Liu, L. Tan, Y. Chen, *Adv. Funct. Mater.* **2017**, *27*, 1703061; c) M. Jung, S. G. Ji, G. Kim, S. I. Seok, *Chem. Soc. Rev.* **2019**, *48*, 2011.

[18] a) W. Li, J. Fan, J. Li, Y. Mai, L. Wang, *J. Am. Chem. Soc.* **2015**, *137*, 10399; b) J.-Y. Seo, J. Matsui, J. Luo, J.-P. Correa-Baena, F. Giordano, M. Saliba, K. Schenk, A. Ummadisingu, K. Domanski, M. Hadadian, A. Hagfeldt, S. M. Zakeeruddin, U. Steiner, M. Grätzel, A. Abate, *Adv. Energy Mater.* **2016**, *6*, 1600767.

[19] a) B. Li, M. J. Li, C. B. Fei, G. Z. Cao, J. J. Tian, *J. Mater. Chem. A* **2017**, *5*, 24168; b) D.-N. Jeong, D.-K. Lee, S. Seo, S. Y. Lim, Y. Zhang, H. Shin, H. Cheong, N.-G. Park, *ACS Energy Lett.* **2019**, *4*, 1189; c) W. Zhou, D. Li, Z. Xiao, Z. Wen, M. Zhang, W. Hu, X. Wu, M. Wang, W. H. Zhang, Y. Lu, S. Yang, S. Yang, *Adv. Funct. Mater.* **2019**, *29*, 1901026.

[20] Z. Liu, J. Hu, H. Jiao, L. Li, G. Zheng, Y. Chen, Y. Huang, Q. Zhang, C. Shen, Q. Chen, H. Zhou, *Adv. Mater.* **2017**, *29*, 1606774.

[21] D. H. Kim, J. Park, Z. Li, M. Yang, J.-S. Park, I. J. Park, J. Y. Kim, J. J. Berry, G. Rumbles, K. Zhu, *Adv. Mater.* **2017**, *29*, 1606831.

[22] a) D. Bi, W. Tress, M. I. Dar, P. Gao, J. Luo, C. Renevier, K. Schenk, A. Abate, F. Giordano, J. P. Correa Baena, J. D. Decoppet, S. M. Zakeeruddin, M. K. Nazeeruddin, M. Gratzel, A. Hagfeldt, *Sci. Adv.* **2016**, *2*, e1501170; b) M. Saliba, T. Matsui, J.-Y. Seo, K. Domanski, J.-P. Correa-Baena, M. K. Nazeeruddin, S. M. Zakeeruddin, W. Tress, A. Abate, A. Hagfeldt, M. Grätzel, *Energy Environ. Sci.* **2016**, *9*, 1989; c) T. Bu, X. Liu, Y. Zhou, J. Yi, X. Huang, L. Luo, J. Xiao, Z. Ku, Y. Peng, F. Huang, Y.-B. Cheng, J. Zhong, *Energy Environ. Sci.* **2017**, *10*, 2509; d) L. Li, N. Liu, Z. Xu, Q. Chen, X. Wang, H. Zhou, *ACS Nano* **2017**, *11*, 8804.

[23] a) Z. Tang, A. M. Guloy, *J. Am. Chem. Soc.* **1999**, *121*, 452; b) C. Colón, A. Alonso-Medina, *Can. J. Phys.* **2001**, *79*, 999; c) H. Miyamae, H. Toriyama, T. Abe, G. Hihara, M. Nagata, *Acta Crystallogr., Sect. C: Cryst. Struct. Commun.* **1984**, *40*, 1559; d) J. Parr, *Polyhedron* **1997**, *16*, 551.

[24] a) K. G. Stamplecoskie, J. S. Manser, P. V. Kamat, *Energy Environ. Sci.* **2015**, *8*, 208; b) J. C. Hamill, J. Schwartz, Y.-L. Loo, *ACS Energy Lett.* **2018**, *3*, 92.

[25] O. E. Lanford, S. J. Kiehl, *J. Am. Chem. Soc.* **1941**, *63*, 667.

[26] K. Yan, M. Long, T. Zhang, Z. Wei, H. Chen, S. Yang, J. Xu, *J. Am. Chem. Soc.* **2015**, *137*, 4460.

[27] R. J. Stewart, C. Grieco, A. V. Larsen, G. S. Doucette, J. B. Asbury, *J. Phys. Chem. C* **2016**, *120*, 12392.

[28] a) R. Munir, A. D. Sheikh, M. Abdelsamie, H. Hu, L. Yu, K. Zhao, T. Kim, O. E. Tall, R. Li, D. M. Smilgies, A. Amassian, *Adv. Mater.* **2017**, *29*, 1604113; b) Q. Hu, L. Zhao, J. Wu, K. Gao, D. Luo, Y. Jiang, Z. Zhang, C. Zhu, E. Schaible, A. Hexemer, C. Wang, Y. Liu, W. Zhang, M. Gratzel, F. Liu, T. P. Russell, R. Zhu, Q. Gong, *Nat. Commun.* **2017**, *8*, 15688.

[29] A. Sharenko, C. Mackeen, L. Jewell, F. Bridges, M. F. Toney, *Chem. Mater.* **2017**, *29*, 1315.

[30] a) W. S. Yang, B. W. Park, E. H. Jung, N. J. Jeon, Y. C. Kim, D. U. Lee, S. S. Shin, J. Seo, E. K. Kim, J. H. Noh, S. I. Seok, *Science* **2017**, *356*, 1376; b) D. Meggiolaro, S. G. Motti, E. Mosconi, A. J. Barker, J. Ball, C. Andrea Riccardo Perini, F. Deschler, A. Petrozza, F. De Angelis, *Energy Environ. Sci.* **2018**, *11*, 702; c) G. Nan, X. Zhang, M. Abdi-Jalebi, Z. Andaji-Garmaroudi, S. D. Stranks, G. Lu, D. Beljonne, *Adv. Energy Mater.* **2018**, *8*, 1702754; d) B. W. Park, N. Kedem, M. Kulbak, D. Y. Lee, W. S. Yang, N. J. Jeon, J. Seo, G. Kim, K. J. Kim, T. J. Shin, G. Hodes, D. Cahen, S. I. Seok, *Nat. Commun.* **2018**, *9*, 3301.

[31] Z. Arain, C. Liu, Y. Yang, M. Mateen, Y. Ren, Y. Ding, X. Liu, Z. Ali, M. Kumar, S. Dai, *Sci. China Mater.* **2019**, *62*, 161.

[32] N. K. Noel, S. N. Habisreutinger, B. Wenger, M. T. Klug, M. T. Hörantner, M. B. Johnston, R. J. Nicholas, D. T. Moore, H. J. Snaith, *Energy Environ. Sci.* **2017**, *10*, 145.

[33] a) G. Akerlof, *J. Am. Chem. Soc.* **1932**, *54*, 4125; b) W. G. Gorman, G. D. Hall, *J. Pharm. Sci.* **1964**, *53*, 1017; c) S. C. Moldoveanu, V. David, in *Essentials in Modern HPLC Separations*, Elsevier, New York **2013**, p. 363; d) S. C. Moldoveanu, V. David, in *Essentials in Modern HPLC Separations*, Elsevier, New York **2013**, p. 115.

[34] V. Gutmann, *Coord. Chem. Rev.* **1976**, *18*, 225.

[35] a) M. I. Saidaminov, A. L. Abdelhady, B. Murali, E. Alarousu, V. M. Burlakov, W. Peng, I. Dursun, L. Wang, Y. He, G. Maculan, A. Goriely, T. Wu, O. F. Mohammed, O. M. Bakr, *Nat. Commun.* **2015**, *6*, 7586; b) J. M. Kadro, K. Nonomura, D. Gachet, M. Grätzel, A. Hagfeldt, *Sci. Rep.* **2015**, *5*, 11654.

[36] M. De Bastiani, M. I. Saidaminov, I. Dursun, L. Sinatra, W. Peng, U. Buttner, O. F. Mohammed, O. M. Bakr, *Chem. Mater.* **2017**, *29*, 3367.

[37] a) M. Ozaki, A. Shimazaki, M. Jung, Y. Nakaike, N. Maruyama, S. Yakumaru, A. I. Rafieh, T. Sasamori, N. Tokitoh, P. Ekanayake, Y. Murata, R. Murdey, A. Wakamiya, *Angew. Chem., Int. Ed. Engl.* **2019**, *58*, 9389; b) A. Ng, Z. Ren, H. Hu, P. W. K. Fong, Q. Shen, S. H. Cheung, P. Qin, J. W. Lee, A. B. Djurisic, S. K. So, G. Li, Y. Yang, C. Surya, *Adv. Mater.* **2018**, *30*, 1804402.

[38] a) Y. Bai, S. Xiao, C. Hu, T. Zhang, X. Meng, Q. Li, Y. Yang, K. S. Wong, H. Chen, S. Yang, *Nano Energy* **2017**, *34*, 58; b) D. Shen, X. Yu, X. Cai, M. Peng, Y. Ma, X. Su, L. Xiao, D. Zou, *J. Mater. Chem. A* **2014**, *2*, 20454.

[39] K. H. Hendriks, J. J. van Franeker, B. J. Bruijnaers, J. A. Anta, M. M. Wienk, R. A. J. Janssen, *J. Mater. Chem. A* **2017**, *5*, 2346.

[40] A. A. Petrov, I. P. Sokolova, N. A. Belich, G. S. Peters, P. V. Dorovatovskii, Y. V. Zubavichus, V. N. Khrustalev, A. V. Petrov, M. Grätzel, E. A. Goodilin, A. B. Tarasov, *J. Phys. Chem. C* **2017**, *121*, 20739.

[41] Z. Xu, Z. Liu, N. Li, G. Tang, G. Zheng, C. Zhu, Y. Chen, L. Wang, Y. Huang, L. Li, N. Zhou, J. Hong, Q. Chen, H. Zhou, *Adv. Mater.* **2019**, *31*, 1900390.

[42] a) D.-Y. Son, J.-W. Lee, Y. J. Choi, I.-H. Jang, S. Lee, P. J. Yoo, H. Shin, N. Ahn, M. Choi, D. Kim, N.-G. Park, *Nat. Energy* **2016**, *1*, 16081; b) Q. Jiang, Z. Chu, P. Wang, X. Yang, H. Liu, Y. Wang, Z. Yin, J. Wu, X. Zhang, J. You, *Adv. Mater.* **2017**, *29*, 1703852.

[43] Q. Chen, H. Zhou, T. B. Song, S. Luo, Z. Hong, H. S. Duan, L. Dou, Y. Liu, Y. Yang, *Nano Lett.* **2014**, *14*, 4158.

[44] a) T. Matsui, T. Yamamoto, T. Nishihara, R. Morisawa, T. Yokoyama, T. Sekiguchi, T. Negami, *Adv. Mater.* **2019**, *31*, 1806823; b) J. P. Correa-Baena, Y. Luo, T. M. Brenner, J. Snaider, S. Sun, X. Li, M. A. Jensen, N. T. P. Hartono, L. Nienhaus, S. Wieghold, J. R. Poindexter, S. Wang, Y. S. Meng, T. Wang, B. Lai, M. V. Holt, Z. Cai, M. G. Bawendi, L. Huang, T. Buonassisi, D. P. Fenning, *Science* **2019**, *363*, 627.

[45] a) A. R. Pascoe, Q. Gu, M. U. Rothmann, W. Li, Y. Zhang, A. D. Scully, X. Lin, L. Spiccia, U. Bach, Y.-B. Cheng, *Sci. China Mater.* **2017**, *60*, 617; b) D. Liu, W. Zhou, H. Tang, P. Fu, Z. Ning, *Sci. China: Chem.* **2018**, *61*, 1278.

[46] B. Conings, A. Babayigit, M. T. Klug, S. Bai, N. Gauquelin, N. Sakai, J. T. Wang, J. Verbeeck, H. G. Boyen, H. J. Snaith, *Adv. Mater.* **2016**, *28*, 10701.

[47] X. Li, D. Bi, C. Yi, J.-D. Décoppet, J. Luo, S. M. Zakeeruddin, A. Hagfeldt, M. Grätzel, *Science* **2016**, *353*, 58.

[48] M. Li, B. Li, G. Cao, J. Tian, *J. Mater. Chem. A* **2017**, *5*, 21313.

[49] a) F. Huang, M. Li, P. Siffalovic, G. Cao, J. Tian, *Energy Environ. Sci.* **2019**, *12*, 518; b) Z. Li, T. R. Klein, D. H. Kim, M. Yang, J. J. Berry, M. F. A. M. van Hest, K. Zhu, *Nat. Rev. Mater.* **2018**, *3*, 18017.

[50] W. Nie, H. Tsai, R. Asadpour, J.-C. Blancon, A. J. Neukirch, G. Gupta, J. J. Crochet, M. Chhowalla, S. Tretiak, M. A. Alam, *Science* **2015**, *347*, 522.

[51] S. Sanchez, X. Hua, N. Phung, U. Steiner, A. Abate, *Adv. Energy Mater.* **2018**, *8*, 1702915.

[52] a) P. Wang, Y. Wu, B. Cai, Q. Ma, X. Zheng, W. H. Zhang, *Adv. Funct. Mater.* **2019**, 1807661; b) L. Qiu, S. He, L. K. Ono, S. Liu, Y. Qi, *ACS Energy Lett.* **2019**, *4*, 2147.

[53] M. He, B. Li, X. Cui, B. Jiang, Y. He, Y. Chen, D. O'Neil, P. Szymanski, M. A. Ei-Sayed, J. Huang, Z. Lin, *Nat. Commun.* **2017**, *8*, 16045.

[54] Y. Zhong, R. Munir, J. Li, M.-C. Tang, M. R. Niazi, D.-M. Smilgies, K. Zhao, A. Amassian, *ACS Energy Lett.* **2018**, *3*, 1078.

[55] Y. Li, Z. Zhao, F. Lin, X. Cao, X. Cui, J. Wei, *Small* **2017**, *13*, 1604125.

[56] a) Y. Ren, B. Duan, Y. Xu, Y. Huang, Z. Li, L. Hu, T. Hayat, H. Wang, J. Zhu, S. Dai, *Sci. China Mater.* **2017**, *60*, 392; b) H. Zhang, M. K. Nazeeruddin, W. C. H. Choy, *Adv. Mater.* **2019**, *31*, 1805702.

[57] a) E. Doni, G. Grosso, G. Harbeke, E. Meier, E. Tosatti, *Phys. Status Solidi B* **1975**, *68*, 569; b) J. Sergio Casas, J. Sordo, M. J. Vidarte, in *Lead: Chemistry, Analytical Aspects, Environmental Impact and Health Effects*, Elsevier, New York **2006**, p. 41.

[58] I. Wharf, T. Gramstad, R. Makhija, M. Onyszchuk, *Can. J. Chem.* **1976**, *54*, 3430.

[59] a) J. W. Lee, H. S. Kim, N. G. Park, *Acc. Chem. Res.* **2016**, *49*, 311; b) T. Niu, J. Lu, R. Munir, J. Li, D. Barrit, X. Zhang, H. Hu, Z. Yang, A. Amassian, K. Zhao, S. F. Liu, *Adv. Mater.* **2018**, *30*, 1706576; c) H. Dong, Z. Wu, J. Xi, X. Xu, L. Zuo, T. Lei, X. Zhao, L. Zhang, X. Hou, A. K. Y. Jen, *Adv. Funct. Mater.* **2018**, *28*, 1704836; d) N. Li, S. Tao, Y. Chen, X. Niu, C. K. Onwudinanti, C. Hu, Z. Qiu, Z. Xu, G. Zheng, L. Wang, Y. Zhang, L. Li, H. Liu, Y. Lun, J. Hong, X. Wang, Y. Liu, H. Xie, Y. Gao, Y. Bai, S. Yang, G. Brocks, Q. Chen, H. Zhou, *Nat. Energy* **2019**, *4*, 408; e) M. Qin, K. Tse, T. K. Lau, Y. Li, C. J. Su, G. Yang, J. Chen, J. Zhu, U. S. Jeng, G. Li, H. Chen, X. Lu, *Adv. Mater.* **2019**, *31*, e1901284.

[60] G. Yin, H. Zhao, H. Jiang, S. Yuan, T. Niu, K. Zhao, Z. Liu, S. F. Liu, *Adv. Funct. Mater.* **2018**, *28*, 1803269.

[61] B. Li, C. Fei, K. Zheng, X. Qu, T. Pullerits, G. Cao, J. Tian, *J. Mater. Chem. A* **2016**, *4*, 17018.

[62] Y. Xia, C. Ran, Y. Chen, Q. Li, N. Jiang, C. Li, Y. Pan, T. Li, J. Wang, W. Huang, *J. Mater. Chem. A* **2017**, *5*, 3193.

[63] Y. Chen, Y. Zhao, Z. Liang, *Chem. Mater.* **2015**, *27*, 1448.

[64] M. S. Yin, F. X. Xie, H. Chen, X. D. Yang, F. Ye, E. B. Bi, Y. Z. Wu, M. T. Cai, L. Y. Han, *J. Mater. Chem. A* **2016**, *4*, 8548.

[65] G. W. P. Adhyaksa, S. Brittman, H. Abolins, A. Lof, X. Li, J. D. Keelor, Y. Luo, T. Duevski, R. M. A. Heeren, S. R. Ellis, D. P. Fenning, E. C. Garnett, *Adv. Mater.* **2018**, *30*, 1804792.

[66] W. Zhang, M. Saliba, D. T. Moore, S. K. Pathak, M. T. Horantner, T. Stergiopoulos, S. D. Stranks, G. E. Eperon, J. A. Alexander-Webber, A. Abate, A. Sadhanala, S. Yao, Y. Chen, R. H. Friend, L. A. Estroff, U. Wiesner, H. J. Snaith, *Nat. Commun.* **2015**, *6*, 6142.

[67] a) Z. Xiao, Q. Dong, C. Bi, Y. Shao, Y. Yuan, J. Huang, *Adv. Mater.* **2014**, *26*, 6503; b) S. Xiao, Y. Bai, X. Meng, T. Zhang, H. Chen, X. Zheng, C. Hu, Y. Qu, S. Yang, *Adv. Funct. Mater.* **2017**, *27*, 1604944.

[68] Y. C. Zheng, S. Yang, X. Chen, Y. Chen, Y. Hou, H. G. Yang, *Chem. Mater.* **2015**, *27*, 5116.

[69] M. Yang, T. Zhang, P. Schulz, Z. Li, G. Li, D. H. Kim, N. Guo, J. J. Berry, K. Zhu, Y. Zhao, *Nat. Commun.* **2016**, *7*, 12305.

[70] a) P. W. Voorhees, *J. Stat. Phys.* **1985**, *38*, 231; b) A. Baldan, *J. Mater. Sci.* **2002**, *37*, 2171.

[71] a) Q. Zhang, S.-J. Liu, S.-H. Yu, *J. Mater. Chem.* **2009**, *19*, 191; b) J. Zhang, F. Huang, Z. Lin, *Nanoscale* **2010**, *2*, 18.

[72] T. W. Kim, S. Uchida, T. Matsushita, L. Cojocaru, R. Jono, K. Kimura, D. Matsubara, M. Shirai, K. Ito, H. Matsumoto, T. Kondo, H. Segawa, *Adv. Mater.* **2018**, *30*, 1705230.

[73] a) M. Saliba, J.-P. Correa-Baena, C. M. Wolff, M. Stolterfoht, N. Phung, S. Albrecht, D. Neher, A. Abate, *Chem. Mater.* **2018**, *30*, 4193; b) M. Saliba, T. Matsui, K. Domanski, J. Y. Seo, A. Ummadisingu, S. M. Zakeeruddin, J. P. Correa-Baena, W. R. Tress, A. Abate, A. Hagfeldt, M. Gratzel, *Science* **2016**, *354*, 206; c) D. Luo, W. Yang, Z. Wang, A. Sadhanala, Q. Hu, R. Su, R. Shivanna, G. F. Trindade, J. F. Watts, Z. Xu, T. Liu, K. Chen, F. Ye, P. Wu, L. Zhao, J. Wu, Y. Tu, Y. Zhang, X. Yang, W. Zhang, R. H. Friend, Q. Gong, H. J. Snaith, R. Zhu, *Science* **2018**, *360*, 1442.

[74] A. Rajagopal, K. Yao, A. K. Jen, *Adv. Mater.* **2018**, *30*, 1800455.

[75] M. Wang, B. Li, P. Siffalovic, L.-C. Chen, G. Cao, J. Tian, *J. Mater. Chem. A* **2018**, *6*, 15386.

[76] S. Tang, Y. Deng, X. Zheng, Y. Bai, Y. Fang, Q. Dong, H. Wei, J. Huang, *Adv. Energy Mater.* **2017**, *7*, 1700302.

[77] Y. Deng, X. Zheng, Y. Bai, Q. Wang, J. Zhao, J. Huang, *Nat. Energy* **2018**, *3*, 560.

[78] J. Lee, J. Yang, S. G. Kwon, T. Hyeon, *Nat. Rev. Mater.* **2016**, *1*, 16034.

[79] S. Pratap, E. Keller, P. Muller-Buschbaum, *Nanoscale* **2019**, *11*, 3495.

[80] B. Li, F. H. Isikgor, H. Coskun, J. Ouyang, *Angew. Chem., Int. Ed.* **2017**, *56*, 16073.

[81] J. S. Manser, B. Reid, P. V. Kamat, *J. Phys. Chem. C* **2015**, *119*, 17065.

[82] a) H. Tsai, W. Nie, Y.-H. Lin, J. C. Blancon, S. Tretiak, J. Even, G. Gupta, P. M. Ajayan, A. D. Mohite, *Adv. Energy Mater.* **2017**, *7*, 1602159; b) D. P. McMeekin, Z. Wang, W. Rehman, F. Pulvirenti, J. B. Patel, N. K. Noel, M. B. Johnston, S. R. Marder, L. M. Herz, H. J. Snaith, *Adv. Mater.* **2017**, *29*, 1607039; c) C. Fei, M. Zhou, J. Ogle, D.-M. Smilgies, L. Whittaker-Brooks, H. Wang, *J. Mater. Chem. A* **2019**, https://doi.org/10.1039/c9ta01755k.

[83] P. Boonmongkolras, D. Kim, E. M. Alhabshi, I. Gereige, B. Shin, *RSC Adv.* **2018**, *8*, 21551.

[84] a) H. Tan, A. Jain, O. Voznyy, X. Lan, F. P. Garcia de Arquer, J. Z. Fan, R. Quintero-Bermudez, M. Yuan, B. Zhang, Y. Zhao, F. Fan, P. Li, L. N. Quan, Y. Zhao, Z. H. Lu, Z. Yang, S. Hoogland, E. H. Sargent, *Science* **2017**, *355*, 722; b) X. Liu, L. Shi, J. Huang, Z. Liu, P. Zhang, J. S. Yun, A. M. Soufiani, J. Seidel, K. Sun, Z. Hameiri, J. A. Stride, Y. Zhang, M. A. Green, H. Lin, X. Hao, *Sol. RRL* **2019**, *3*, 1800338.

[85] Z. M. Zhou, Z. W. Wang, Y. Y. Zhou, S. P. Pang, D. Wang, H. X. Xu, Z. H. Liu, N. P. Padture, G. L. Cui, *Angew. Chem., Int. Ed.* **2015**, *54*, 9705.

[86] H. Chen, F. Ye, W. Tang, J. He, M. Yin, Y. Wang, F. Xie, E. Bi, X. Yang, M. Gratzel, L. Han, *Nature* **2017**, *550*, 92.

[87] L. Chao, Y. Xia, B. Li, G. Xing, Y. Chen, W. Huang, *Chem* **2019**, *5*, 995.

[88] M. Qin, J. Cao, T. Zhang, J. Mai, T.-K. Lau, S. Zhou, Y. Zhou, J. Wang, Y.-J. Hsu, N. Zhao, J. Xu, X. Zhan, X. Lu, *Adv. Energy Mater.* **2018**, *8*, 1703399.

[89] B. Dou, L. M. Wheeler, J. A. Christians, D. T. Moore, S. P. Harvey, J. J. Berry, F. S. Barnes, S. E. Shaheen, M. F. A. M. van Hest, *ACS Energy Lett.* **2018**, *3*, 979.

[90] W. Zhang, S. Pathak, N. Sakai, T. Stergiopoulos, P. K. Nayak, N. K. Noel, A. A. Haghighirad, V. M. Burlakov, D. W. deQuilettes, A. Sadhanala, W. Li, L. Wang, D. S. Ginger, R. H. Friend, H. J. Snaith, *Nat. Commun.* **2015**, *6*, 10030.